

Research Paper

Colloids, nanoparticles, and materials for imaging, delivery, ablation, and theranostics by focused ultrasound (FUS)

Adem Yildirim^{1,2,✉}, Nicholas T. Blum,¹ and Andrew P. Goodwin^{1,✉}

1. Department of Chemical and Biological Engineering, University of Colorado Boulder, Boulder, CO 80303 USA

2. Present address: CEDAR, Knight Cancer Institute, Oregon Health and Science University, Portland, OR, 97239 USA

✉ Corresponding authors: andrew.goodwin@colorado.edu; adem.yildirim@colorado.edu

© Ivyspring International Publisher. This is an open access article distributed under the terms of the Creative Commons Attribution (CC BY-NC) license (<https://creativecommons.org/licenses/by-nc/4.0/>). See <http://ivyspring.com/terms> for full terms and conditions.

Received: 2018.12.19; Accepted: 2019.03.25; Published: 2019.04.13

Abstract

This review focuses on different materials and contrast agents that sensitize imaging and therapy with Focused Ultrasound (FUS). At high intensities, FUS is capable of selectively ablating tissue with focus on the millimeter scale, presenting an alternative to surgical intervention or management of malignant growth. At low intensities, FUS can be also used for other medical applications such as local delivery of drugs and blood brain barrier opening (BBBO). Contrast agents offer an opportunity to increase selective acoustic absorption or facilitate destructive cavitation processes by converting incident acoustic energy into thermal and mechanical energy. First, we review the history of FUS and its effects on living tissue. Next, we present different colloidal or nanoparticulate approaches to sensitizing FUS, for example using microbubbles, phase-shift emulsions, hollow-shelled nanoparticles, or hydrophobic silica surfaces. Exploring the science behind these interactions, we also discuss ways to make stimulus-responsive, or “turn-on” contrast agents for improved selectivity. Finally, we discuss acoustically-active hydrogels and membranes. This review will be of interest to those working in materials who wish to explore new applications in acoustics and those in acoustics who are seeking new agents to improve the efficacy of their approaches.

1. Introduction

Ultrasound waves generated by an acoustic transducer can be focused into a small volume using, usually, a concave shaped or phased array transducer. At the focal zone, which is about the size of an uncooked grain of rice, the acoustic intensity is orders of magnitude higher than the intensity at the surface of the transducer. This, together with the high penetration depth of ultrasound in soft tissue, enables site-selective delivery of relatively high acoustic intensities into a small target volume in the body without significantly affecting the tissue on the path of ultrasound [1]. Depending on the acoustic intensity, temperature increase and/or cavitation can be induced in the focal zone, which can result in various effects in the tissue from mild hyperthermia

to coagulative necrosis and transient poration of the cell membrane to mechanical tissue ablation [2–4]. One of the most common uses of focused ultrasound (FUS) in medicine is the thermal ablation of a target tissue, which leverages from the rapid temperature increase in the tissue at high acoustic intensities to induce coagulative necrosis [2,5–9]. This process is usually called High Intensity Focused Ultrasound (HIFU) therapy or ablation. FUS can also be used to mechanically fractionate the tissue by applying FUS pulses with higher acoustic pressures [4,10,11]. By moving the focal zone of FUS, larger volumes (>cm³) can be ablated or fractionated with millimeter precision [1]. Owing to the excellent penetration depth of the high intensity ultrasound pulses in soft

tissue, FUS, or more specifically HIFU, is promising for non-invasive ablation of soft-tissue such as solid tumors or brain tissue [2,6]. While high scattering of ultrasound from interfaces of tissue with gas or bone partially limits the clinical application of HIFU [2], it has been successfully applied to ablate several malignant or benign diseases located superficially or deep in the body, including uterine fibroids as well as tumors found in the prostate, breast, and, liver, and brain (transcranial) [1,6–8]. Thus, HIFU is a promising alternative to invasive surgery and may offer greater precision, decreased morbidity, and mortality rates with lower treatment cost and shorter recovery times [1]. FUS has also been used for on-demand and spatially-controlled drug delivery. In this case, FUS pulses with lower intensities is applied for improving the local delivery of drugs and genes by inducing mild hyperthermia in the tissue, and/or by mechanically creating temporary pores in the cell membranes and blood brain barrier (BBB) [3,12].

However, the therapeutic outcomes of current FUS therapies are still unsatisfactory [13,14]. For instance, thermally ablated solid tumors often recur, and the high pressure requirement for mechanical tissue fractionation or trans-cranial applications can induce off-target damage in the healthy tissue [15,16]. To both increase FUS efficacy and reduce the pressure requirement for tissue damage, ultrasound contrast agents such as fluorocarbon microbubbles and nanodroplets or gas-stabilizing nanoparticles have been utilized to locally enhance thermal and mechanical effects induced by FUS treatment and, thus, enable a more precise, efficient, and safer ablation of the soft tissue [17–23]. Such ultrasound active materials have also been applied for several other applications, including drug delivery, ultrasound imaging, and blood brain barrier opening (BBBO) [24–31]. In this review, we will first briefly summarize the history of FUS and its principles. Then, we will comprehensively summarize the different types of ultrasound active materials developed for FUS theranostics. Finally, we will conclude by discussing the current limitations and potential future directions in the field.

2. History of Focused Ultrasound and Its Instrumentation

Despite the many recent technological advances in generating high intensity ultrasound waves and their focusing into small volumes, FUS pulses were first generated almost 100 years ago. Piezoelectricity, or the conversion of the mechanical motion to an electrical signal and vice versa, was discovered in 1880 by Jacques and Pierre Curie, which in turn led to the development of sonar devices in the early 1900s

[32,33]. The application of alternating current generated sound waves in the receiving medium, and larger currents meant more intense sound waves [34]. Thus, the early 1900s witnessed the first experiments regarding the effects of high-intensity ultrasound on biological organisms. In particular, Wood and Lomis studied the biological effects of the ultrasound on living organisms in a water tank [35]. They showed that high-intensity ultrasound destroyed red blood cells and killed small fishes and frogs, but bacteria and mice survived after several minutes of insonation. This straightforward experiment proved that ultrasound could cause biological damage at high intensities.

Focusing the ultrasound pulses into a small volume, which further increases the acoustic intensities and pressures by a factor of ~10-100, was experimentally first achieved by Gruetzmacher in 1935 by using a concave shaped quartz crystal lens [36]. Less than a decade later, Lynn, *et al.*, proposed the idea of non-invasive surgery by thermally ablating the tissue in the focal zone, leaving the tissue outside the ablated area mostly unaffected because of the significantly lower acoustic intensities in these regions [37]. This approach successfully created ablated lesions in cat brains [38]. After this initial success, the development in this field slowed for several decades, primarily because of the dearth of imaging modalities that could enable precise focusing and real-time monitoring of the HIFU treatment [39,40]. However, the 1980's saw the developments in transducer design, allowing both focusing and real-time imaging capability of the target tissue using MRI or ultrasound imaging [7,41]. With these advancements in treatment precision, non-invasive HIFU tissue ablation has been tested on several tumors, including pancreatic, breast, bladder, prostate, renal, and liver tumors, along with non-malignant tissues such as brain and uterine fibroids [1,6–8]. Currently, several commercial pieces of HIFU equipment with ultrasound or MR guidance for ablation of prostate and breast tumors, uterine fibroids, bone metastases, and brain tissue are available worldwide [2].

Contemporary FUS instrumentation uses either a bowl-shaped single piezoelectric element or a phased array of transducers (Figure 1A) [2]. Single element and phased array FUS transducers are commercially available that can operate at a broad range of frequencies (0.2 to 20 MHz). These transducers are able to focus the sound into a small, cigar-shaped volume with usually a few mm in diameter and around a cm in length, about the size of an uncooked grain of rice [1]. At the focal zone, these transducers can create very high ultrasound intensities and acoustic pressures up to 100,000 Watts/cm² and 100

MPa, respectively. For focused single element transducers, the focal point is fixed at a geometrically defined point and thus must be moved mechanically during treatment. On the other hand, phased array transducers can be directed electronically to create multiple focal points, but these transducers are costlier than single element transducers. Finally, it is also possible to focus ultrasound generated by a flat transducer using an acoustic lens, which can focus sound waves based on the difference in speed of sound in different media. This design gives flexibility for tuning the position of the focal point but suffers from acoustic losses [39].

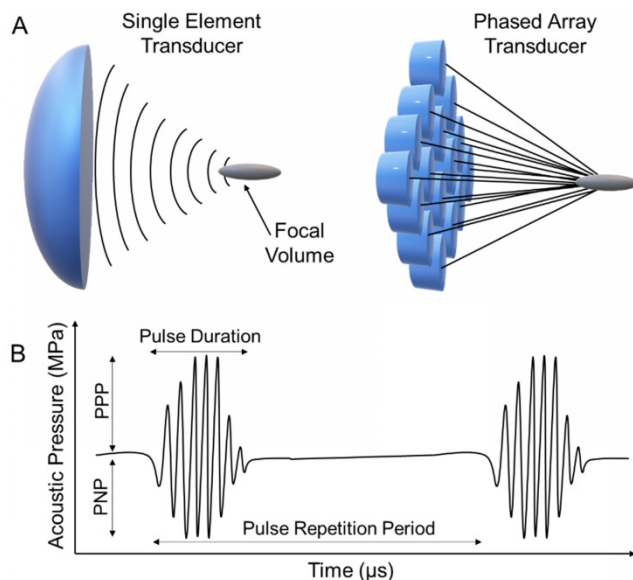


Figure 1. A) Schematic representation of single element and phased array FUS transducers. B) Schematic representation of a typical FUS waveform and the important acoustic parameters.

3. Bioeffects and Applications of FUS.

Ultrasound waves are mechanical waves that cause local positive and negative pressure differences in the receiving medium during propagation [42]. By definition, a sound wave with a frequency (*i. e.*, cycles per second) above the human hearing limit (~ 20 kHz) is termed ultrasound. While there is no set upper limit, theoretically it is not possible to obtain sound waves with frequencies higher than $\sim 10^{13}$ Hz because the wavelength would approach the atomic spacing of a condensed phase medium. In medical ultrasound, the most commonly used frequencies are between 0.1 and 40 MHz. Lower frequencies provide a greater chance of generating bioeffects and are limited in their focusing resolution. On the other hand, the attenuation of ultrasound in soft tissue increases at higher frequencies; while 1 MHz ultrasound waves can be used treatment of ~ 5 cm deep soft tissue, the treatment depth decreases to ~ 2 cm at 3 MHz [43].

For medical FUS, it is common to report both peak negative (or rarefactional) pressure (PNP) and peak positive (or compressional) pressure (PPP) because waveforms become asymmetrical at higher PPPs, especially at high intensities, due to the non-linear propagation effects in soft tissue (Figure 1B). The acoustic pressures of the FUS pulses can be determined by collecting the waveforms using a hydrophone [44–46], with typically the highest positive and negative values in the pressure waveform reported as PPP and PNP, respectively. FUS pulses with PNPs of between ~ 0.1 and 25 MPa are commonly applied for different purposes, and at these conditions, PPP values could reach 100 MPa. Using pressure waveforms, acoustic intensity can be then calculated, which is defined as power per unit area that is carried by sound waves. As the acoustic intensities both temporally and spatially change in a propagating FUS beam, it can be reported in several different ways by considering the average and peak intensities, pulse shape and duration. The most commonly used intensity parameters are spatial-peak pulse-average (I_{SPPA}) and spatial-average temporal-average (I_{SPTA}) (see ref [46] for further information) [47]. I_{SPPA} provides information on the instantaneous pulse intensity, where I_{SPTA} is more useful for determining possible temperature rise and overall acoustic energy input.

Other important FUS parameters include pulse duration and pulse repetition period (PRP) (Figure 1B). FUS is usually applied as pulses at low duty cycle to prevent extreme thermal energy accumulation in the tissue. Pulse duration is determined ideally by the number of waveforms per pulse (also known as cycle number) and the operating frequency of the transducer. However, because most transducers are not perfectly damped, the actual pulse duration can be longer than the theoretically predicted value and should be determined through hydrophone measurements [47]. PRP is the time between the start of each pulse. Pulse repetition frequency (PRF), which is number pulses in a second, can also be reported instead. Finally, the ratio between pulse duration and PRP is used to calculate the duty cycle.

While ultrasound waves propagate through the body, they attenuate through reflection or absorption by tissues, bones, or interfaces. While the former can be used to form conventional B-mode ultrasound images, the latter can cause heating in the tissue. At high acoustic pressures, the ultrasound waves can also cause cavitation events in the tissue or at the interfaces. The extreme pressures and temperatures (above 1000 atm and up to 15,000 K, respectively) generated in the cavitating bubbles can induce mechanical and chemical effects in the tissue, in

addition to tissue heating [2,6,40,48]. The type of predominant bioeffect is dictated by the ultrasound parameters described above (Figure 1B). For example, administration of second-long pulses with lower peak negative pressures (usually 1 to 10 MPa) can cause a rapid temperature increase at the focal zone. Reaching temperatures of 60-95 °C causes almost immediate tissue coagulation and necrosis [1]. This effect serves as the basis of the currently approved HIFU based soft tissue ablation methods [49-51], also known as "thermal HIFU ablation." The overall success of this approach is debatable. While several commercial HIFU devices have been developed, the therapeutic outcomes of this method are still unsatisfactory, especially for the treatment of cancer [13,14]. For example, the heat sink effect, which is a cooling effect due to blood flow, can prevent complete thermal ablation of the target tissue at the locations close to the blood vessels [52]. In addition, at the peripheral to the treatment area, temperature rise may not be sufficiently high to generate coagulative necrosis, and diseased cells in that region can survive from the treatment, eventually leading to recurrence [53]. The overall dosage is limited by safety concerns because tissue heating that occurs due to off-target HIFU or blood flow can be dangerous to the patient. As a result, a significant amount of time (hours) must be devoted to each treatment to avoid nonspecific heating, which in turn increases the cost to the patient [54].

More recently developed transducers can induce mechanical rather than thermal effects in tissue. These effects are obtained by applying very short pulses in the range of microseconds, with very high PNP's (>20 MPa) [4,55]. In this case, the temperature increase in the tissue can be minimized (less than 10 °C) and the high rarefactional pressures can generate cavitating bubbles, which then may form shock waves, water jets, and shear forces [6]. Achieving such mechanical bioeffects is the basis of the method called "histotripsy" or "mechanical HIFU ablation," where the cavitating bubbles cause the mechanical destruction of the tissue [4,56-58]. In addition, an acoustic wave is by itself a mechanical wave, and at high intensities, it also can create adverse bioeffects such as membrane deformation and organelle rotation [2]. Finally, due to the high local pressures and temperatures formed during cavitation events, chemical effects such as reactive oxygen species (ROS) generation can be observed, which induce cytotoxicity by, for example, DNA damage [40]. Generation of these effects in the tissue using sonosensitizing materials (*e. g.* dyes such as porphyrins or titanium dioxide nanoparticles) have been utilized for therapeutic purposes through sonodynamic therapy.

We have not reviewed these materials here because they typically use unfocused, low intensity ultrasound, but more information can be found in the recent review by Chen and coworkers [59].

Because mechanical ablation is not influenced by the heat sink effect, it can theoretically provide a more uniform, efficient, and complete removal of the tissue. However, the cavitation events required to obtain such mechanical effects in the deep tissue are difficult to control or predict. As a result, the probability of generating random cavitation events in the tissue or at tissue interfaces becomes more likely at higher pressures, which can induce side-effects such as skin burn and damage to the neighboring healthy tissue has been observed at high acoustic intensities [2,16]. The FUS treatment is also limited by the focal zone; because a single FUS treatment usually ablates a volume of around 100 mm³, several single shots must be applied to ablate large volumes. To minimize the damage to the surrounding healthy tissue a sufficiently long cooling time between two pulses should be applied for thermal ablation procedures. Therefore, as with thermal ablation, the complete ablation of large volumes can take several hours [1].

In the last few decades, acoustically active micro/nanomaterials such as fluorocarbon microbubbles and nanodroplets have been increasingly applied to ablate larger volumes at single thermal or mechanical HIFU treatment spot [22]. Administration of these materials not only increases the ablated tissue volumes but also could decrease the needed ultrasound intensity for ablation and, thus, lower the temperature rise outside the focus, which could make the HIFU therapy safer [20]. In addition, faster ablation of tissue can be achieved in the presence of such ultrasound active materials [60], which is particularly important in the treatment of large tumors (> 5 cm) that can take several hours using conventional thermal HIFU therapy. Furthermore, strategies to target these ultrasound-active materials to the tissue could improve the efficiency and precision of the ablation.

Beyond ablation, acoustically active materials have been shown utility in other applications, including medical imaging and drug delivery. For example, phase change droplets can be vaporized "on demand" into highly echogenic micron-sized bubbles using FUS pulses, and therefore, they can significantly improve the contrast of ultrasound images [31]. Such materials are also attractive for delivery purposes since it is possible to locally and on-demand deliver drugs at diseased sites following their vaporization by FUS insonation [29]. Using such a strategy, it is also possible to reduce the side effects of the drug by minimizing their off-target release and decreasing the

therapeutic dosage. In addition, the mechanical effects generated because of inertial cavitation of vaporized droplets can help to deliver drugs and nanoparticles deeper in the target tissue.

As a particular case of drug delivery, blood-brain barrier opening (BBBO) using FUS for delivering therapeutics into the brain is also an important research area, and significant research effort has been devoted for developing materials that can address this challenge [61–63]. The blood-brain barrier (BBB) is a composite structure separating and regulating the cerebral interstitium. With the exception of a few small (<400 Da), lipophilic (<8 H-bonds with water) molecules and gases that diffuse across the membrane, the BBB rejects most small molecule drugs in addition to virtually all large molecule therapeutics, which makes treatment of disorders in the central nervous system (CNS) exceedingly difficult [64–66]. FUS by itself has been shown to induce BBBO through a combination of mechanical transduction and mild hyperthermia [66–68]. However, the applied acoustic intensity must be tightly controlled to avoid ablation of brain tissue. With the help of acoustically active materials, a more effective and controlled BBBO could be possible using safer FUS intensities [62,69,70].

Below, we will discuss the major types of acoustically active materials used in FUS theranostics. We will summarize the notable achievements in their design and applications to develop FUS based methods for biomedical applications including tumor ablation, drug delivery, bioimaging, and blood-brain barrier opening.

4. Acoustically Active Materials for FUS Theranostics

4.1. Stabilized Fluorocarbon Microbubbles

Ultrasound contrast agents based on stabilized micron-sized gas cavities (*i.e.*, microbubbles) were initially developed to improve the contrast of the ultrasonograms during the late 1960s and early 1970s [71]. Today, several of them are commercially available and clinically approved in the United States, Europe, Japan, and South Korea [72]. While the original microbubble contrast agents consistent were air bubbles stabilized by a shell of phospholipids, polymers, or proteins, today microbubbles are made with fluorocarbon gases (such as octafluoropropane, decafluorobutane, or pentafluoropentane) that exhibit lower vapor pressures and up to 4 orders of magnitude smaller water solubility compared to air [73]. These bubbles scatter ultrasound waves and thus significantly improve backscattered signal intensity. In addition, under low acoustic intensities they can

stably cavitate (*i.e.*, oscillate nonlinearly) and generate harmonic frequencies, which can be detected by an ultrasound imaging probe [73].

When higher acoustic pressures are applied, the bubble becomes unstable, rapidly growing and then collapsing in a process called inertial cavitation [74]. The violent collapse of the bubble could generate mechanical effects such as shock waves and water jets, and thus could be useful in several FUS based therapies such as HIFU ablation and drug delivery [75,76]. For example, larger ablated lesions were observed when microbubbles were applied with thermal or mechanical HIFU treatment in several studies [77–79]. Beyond tumor ablation, microbubbles have also been successfully applied for other mechanical destruction applications such as ablation of brain tissue, thrombolysis, and therapy of hypertrophic cardiomyopathy [80–82].

A recent study showed that when microbubbles were exposed to relatively low pressures using an unfocused imaging probe, they burst and form nanoparticles that are small enough to be able to extravasate from blood vessels [83]. While the composition and physical state of the formed nanoparticles have not been characterized thoroughly yet, our group showed that when nanoparticle solutions, which are generated by microbubble burst, were treated with HIFU they could form bubbles again and generated ultrasound contrast and cavitation events (Figure 2). To demonstrate that the nanoparticles that formed by the burst of microbubbles could be useful in HIFU therapy, we treated breast cancer cells that were grown in a plastic imaging window (Opticell) and observed complete cell detachment from the surface in the presence of the destroyed microbubbles solutions after HIFU treatment.

Microbubbles have also been extensively studied for drug delivery applications [85]. There are two main strategies in the literature; 1) co-injection of microbubbles and free drugs or drug carriers and induce cavitation events by ultrasound application to improve drug accumulation in the target tissue, and 2) loading the therapeutics into the shells of microbubbles and use ultrasound pulses to burst bubbles to release their loads. As an example of the first strategy, Lin and coworkers injected commercially available microbubbles (SonoVue) to tumor-bearing mice and then insonated the tumors with FUS [86]. Then, they injected liposomes containing a chemotherapy drug, doxorubicin (DOX) and investigated the liposome accumulation in tumors. Higher amounts of DOX was found in the sonicated tumors in the presence of microbubbles. In a recent work, Yeh and coworkers optimized the

ultrasound and bubble parameters to obtain better spatial uniformity in tumor penetration using microbubbles and DOX-loaded liposomes [87]. Coussios and coworkers, on the other hand, used this strategy to enhance the delivery of breast cancer-selective oncolytic adenovirus, AdeEHE2F-Luc, in a tissue-mimicking model [88].

Loading drugs into the shells of microbubbles would enable better spatial control for delivery of the drug to the diseased site and could decrease the side effects associated with a high drug dose. However, due to their low surface area, the attachment or loading therapeutics on the monolayer shells of microbubbles is very limited [89]. To overcome this issue, one way is attaching secondary carriers, such as drug-laden liposomes, to microbubble surfaces [90,91]. Geers et al. showed that 600 to 1300 DOX-loaded liposomes could bound per single microbubble by adding a phospholipid-PEG-maleimide linker to the shells of lipid stabilized microbubbles to conjugate liposomes to the microbubble surface (Figure 3) [92]. This strategy enabled in vitro cancer cell killing at very low DOX concentrations where free DOX has no significant effect on the viability. In addition, Nakatsuka, et al. created composites of lipids and crosslinked polymers, which increased the loading of small molecules on the microbubble shell [89].

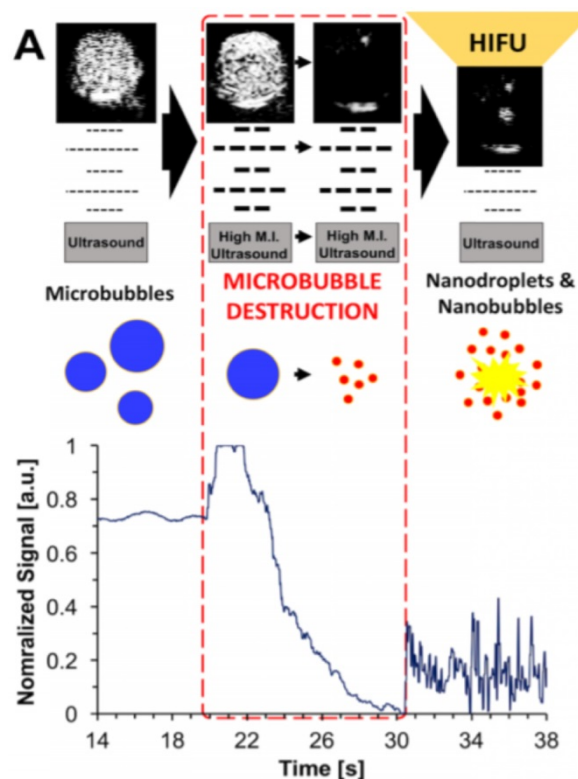


Figure 2. Schematic representation of microbubble destruction and contrast regeneration under HIFU sonication. Adapted from [84], copyright 2017 Ivyspring International Publisher.

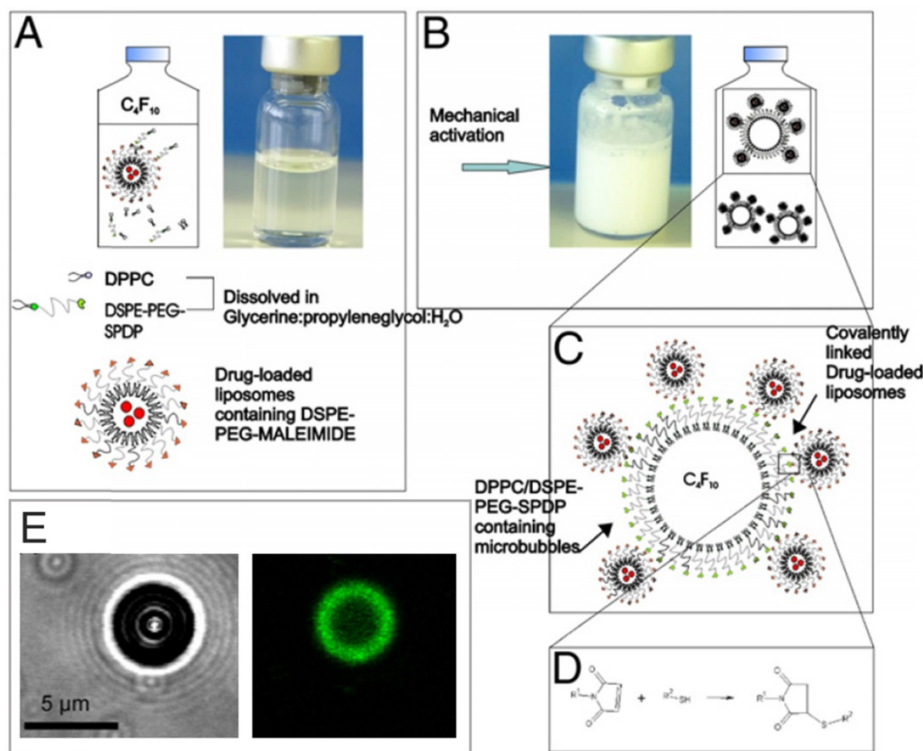


Figure 3. A-D) Schematic showing the details of the preparation of drug loaded liposome attached microbubbles. E) Bright-field (left) and confocal (right) images of a liposome attached microbubble. Liposomes were labelled with a green fluorescent dye. Adapted with permission from [92], copyright 2011 Elsevier.

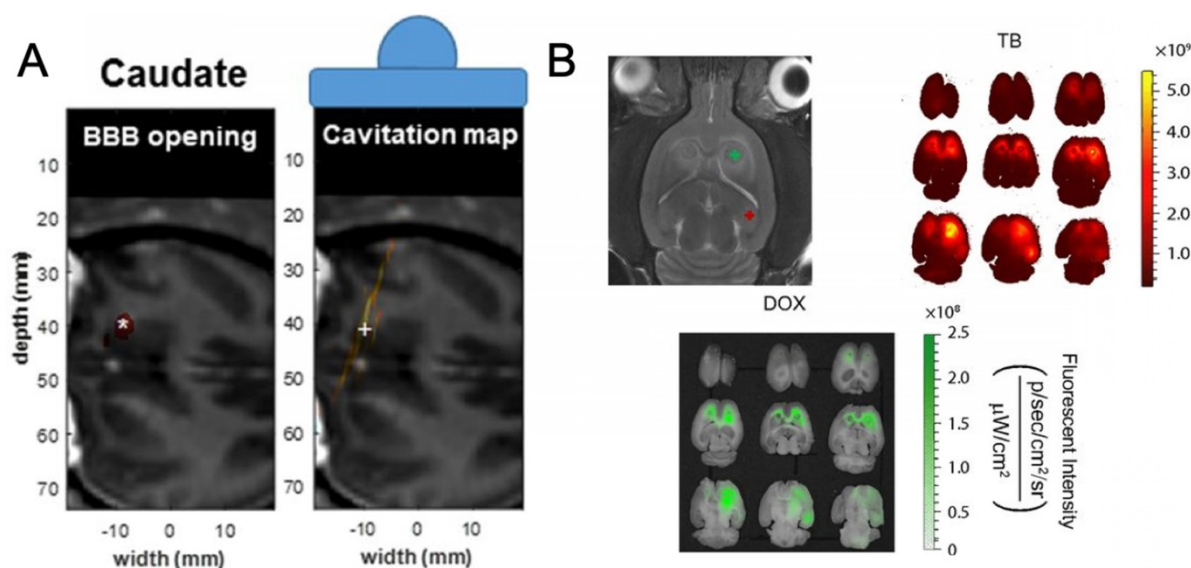


Figure 4. (A) BBBO study in murine model schematic showing (left) targeted area and (middle) representative fluorescent imaging for Trypan Blue and doxorubicin (right). (B) (left) BBBO opening visualization in primate caudate and associated cavitation map (right) with centroids denoted by (*) and (+), respectively. (A) was adapted from reference [113], copyright 2018, Nature Publishing Group. (B) was adapted from reference [114], copyright 2017, National Academy of Sciences.

Administration of microbubbles for enhancement of BBBO by FUS has also been studied by several teams [61,93–97] (Figure 4). Hynynen et al. first showed that, with the addition of microbubbles, one could easily control, by varying the applied ultrasonic power, the effects ranging from no histological alteration of the tissue to complete ablation of the focused area [69]. The parameter space corresponding to a therapeutic BBBO was greatly enlarged. A BBBO phenomenon may be described as "therapeutic" when the BBB is sufficiently disrupted to allow the passage of the therapeutic into the CNS, but not so much as to cause lasting damage to the capillary or brain tissue [68]. The BBB, once reversibly disrupted, will usually restore itself within 24 hours or less [98]. While there is little direct evidence of the biophysical mechanism regarding enhanced permeability of the BBB resulting from microbubble-enhanced FUS disruption, it thought to be a combination of four mechanisms: (1) stimulated transduction across the endothelium, (2) pore or channel formation in the endothelial cells, (3) disruption of tight junctions between the endothelial cells, and (4), at higher intensities, free diffusion through hemorrhaged endothelium [66,99–101]. In the absence of detectable tissue damage it is challenging to determine which pathway is primarily responsible for therapy. Regardless, microbubble-enhanced FUS has proven to be an effective means of BBBO and has been used in the delivery in several types of therapeutics from RNA to synthetic drugs; these and other treatments using microbubbles have already been reviewed in detail by Borden et al. [61,102–107]. It is also possible to deliver nanoparticles to the brain

using a combination of microbubbles and FUS [108–112]. For example, Price and coworkers decorated microbubbles with 150 nm poly(lactic-co-glycolic acid) nanoparticles and observed a two-fold enhancement in the nanoparticle delivery compared to coinjection of free microbubbles and nanoparticles [111,112].

Major limitations of microbubbles include their short in vivo half-lives, often on the order of a couple of minutes, and their large sizes (1–10 μ m), which prevent their accumulation and penetration into the target tissues such as solid tumors [28,115,116]. Also, in the tissue ablation studies, significant heating and damage away from the target were observed since microbubbles are acoustically active throughout the acoustic field, not only at the focal zone [117]. This is because microbubbles require very low acoustic intensities to generate cavitation events [118]. In addition, since microbubbles are such excellent scatterers of ultrasound waves, they can disrupt the focusing of ultrasound waves by scattering them before they reach the area of focus [113,117,119]. This can, for example, allow for the failure of BBBO in the designated area, but may also cause undesired cavitation or possible BBBO in areas of the brain outside the area of focus [113,117,119].

4.2. Phase Change Fluorocarbon Droplets

Phase-change emulsions are condensed fluid droplets stabilized by an amphiphilic shell; in the most typical formulations they use a fluorocarbon core and a lipid stabilizer, but various other stabilizers such as proteins or polymers (e.g., poly(lactic-co-glycolic acid) or poly(ethylene glycol – propylene

glycol – ethylene glycol) have also been used [120]. When a nanodroplet is exposed to sufficiently high acoustic intensities, such as those present at the focal area of a FUS transducer, the volatile core will vaporize (*i. e.* acoustic droplet vaporization; ADV), creating microbubbles and, subsequently cavitation events. Phase-change droplets are more stable than microbubbles because of their liquid core, can be formulated at smaller sizes than bubbles (~ 200 nm to $1 \mu\text{m}$), and exhibit longer half-lives *in vivo* because of their lower solubility and diffusivity. In addition, vaporization of phase-change droplets using external FUS pulses provides better lateral focusing and thus reduces side effects outside the focal zone. For example, Dayton and coworkers compared the efficacy of nanodroplets and microbubbles in improving the HIFU ablated volumes in rat livers [117]. They intravenously injected the nanodroplets or microbubbles and 5, 15, and 95 min after injection they treated the animals with HIFU. According to magnetic resonance thermometry results, significant off-target heating was observed for microbubbles but almost none for nanodroplets. In addition, when the rats were treated with HIFU even after 95 min of injection, significant heating at the focus was observed for nanodroplets, which suggest the better stability of nanodroplets in *in vivo* conditions. In another work by the same group, two droplet compositions, phospholipid-stabilized decafluorobutane (DFB), and octafluoropropane (OFF) droplets were compared with a microbubble ultrasound contrast agent in a rat model [121]. After focused ultrasound vaporization of the droplets, a similar ultrasound contrast to that of microbubbles was observed, with up to 3.3 times longer blood circulation times for droplets depending on composition.

The potential use of ADV for therapeutic purposes was first proposed by Carson and coworkers, who prepared phase-change emulsions by stabilizing dodecafluoropentane (DDFP) droplets using bovine serum albumin [122]. The droplets had a broad size distribution, with 90% of them smaller than $6 \mu\text{m}$. Above a rarefactional acoustic pressure threshold (between 0.8 and 4.5 MPa, depending on the frequency) droplets were vaporized into bubbles with diameters around 25 times larger than their original diameters. They proposed that these droplets might be useful for blood vessel occlusion in cancer treatment. Following this initial study, several fluorocarbon droplet formulations were developed and administered to improve the outcomes of both thermal and mechanical HIFU ablation of the soft tissue (Figure 5) [17,62,123–125]. In one of the early studies Porter et al., also prepared albumin coated

DDFP droplets, but with sizes smaller than 400 nm [123]. They demonstrated that a higher temperature rise could be achieved when the DDFP droplets were applied with HIFU. Several subsequent studies reported larger ablated tumor volumes using fluorocarbon droplets. For example, Li *et al.*, observed significantly larger ablated lesions, at least 3x larger than those obtained with HIFU alone using PLGA stabilized perfluorohexane (PFH) nanodroplets in a rabbit hepatocellular carcinoma model [126]. Clearly, increasing the ablated volume after single HIFU treatment can also decrease ablation time by requiring fewer focal adjustments. Fowlkes and coworkers studied this *in vitro* using tissue-mimicking phantoms and lipid-coated fluorocarbon droplets with average diameters around $2 \mu\text{m}$ [60]. In the presence of phase-change droplets, ablation was 4x faster compared to the conventional thermal HIFU treatment.

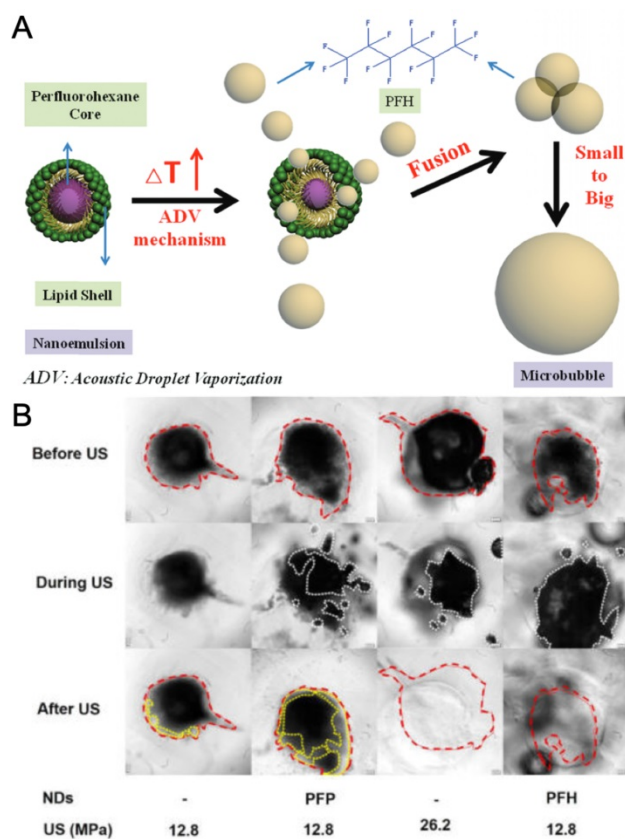


Figure 5. A) Illustration of the nanodroplets and the droplet vaporization process. B) Mechanical ablation of PC-3 prostate cancer spheroids using PFP or PFH nanodroplets at different acoustic pressures. A is adapted from reference [17], copyright 2013 Wiley-VCH. B is reproduced from reference [127], copyright 2016 American Chemical Society.

Phase-change droplets have also been applied to improve the outcomes of mechanical HIFU therapy [57,127–129]. As mentioned in Section 3, a significant limitation of this method is the requirement of high acoustic pressures to generate cavitation events in the

target tissue, which is difficult to deliver safely and effectively into deep tissue. Administration of phase-change droplets can significantly reduce the acoustic cavitation threshold. The laboratories of Zhen Xu and Mohamed El-Sayed had demonstrated that mechanical damage in tissue-mimicking phantoms could be achieved at peak negative pressures as low as ~13 MPa in the presence of amphiphilic triblock polymer stabilized nanodroplets, where no or very little damage was observed when only HIFU was applied [57,127,128]. Hynynen et al., showed that acoustic intensities needed for blood clot lysis could be reduced in the presence of fluoro-surfactant stabilized DDFP droplets [130]. Blood clots were formed in rabbit brains and insonated with HIFU at acoustic intensities of between 88 and 137 W. Compared to a previous study, in which blood clot lysis was achieved by using only HIFU treatment, they observed that the blood clots formed in rabbit brains could be lysed at around four times lower acoustic intensities [131]. In contrast, Yeh and coworkers studied the mechanical effects of the ADV process on vasculature using an in vitro agarose phantom model [132]. Erosion at the walls of the vessel phantom due to the cavitation events generated by the fluorocarbon droplet vaporization was observed at peak negative pressures as low as 10 MPa.

One concern with clot lysis using FUS is the distal occlusions due to the release of large blood clot particles [133–135]. Even beyond more urgent risks like embolism, microemboli have been linked to nefarious long-term effects such as depression and migraine headaches [136]. Thus, study of the post-FUS clot particulates is important for reducing the risk of such emboli and thus should be a standard method for evaluating clot lysis in vitro [137–140]. Thus, we believe that by tuning the acoustic parameters of FUS and correct selection of the acoustically active material and its concentration a safe treatment window should be achieved.

FUS activated phase-change droplets have been applied as contrast agents for the ultrasound and photoacoustic imaging. Acoustic vaporization of phase-change droplets was first proposed for correcting aberrations in ultrasound imaging and improving the contrast of ultrasonograms [122,141,142]. For example, Kripfgans and coworkers used micron-sized DDFP droplets for transcranial ultrasound aberration correction [143]. Acoustically vaporized droplets were used as point targets to correct the aberrations in transcranial ultrasound images, where aberration caused by the skull is a significant limitation. It is important to note that nanodroplet concentration should be low when applied for imaging purposes to reduce the

mechanical damage caused by inertial cavitation events [122].

As it is possible to prepare phase change droplets in the sub-micrometer range, they have been long recognized as potential extravascular contrast agents for cancer imaging [31]. Their smaller size makes their escape from leaky tumor vasculature and accumulation in the tumor microenvironment possible through the enhanced permeability and retention (EPR) effect [144,145]. For example, Li et al., prepared folate-targeted nanodroplets and showed that the nanodroplets could enhance tumor imaging in mouse models when they were vaporized using low intensity FUS (LIFU) [146].

Phase-change droplets have also been applied to improve the contrast of the photoacoustic images. In a recent study, Pozzo et al. developed polypyrrole (PPy) doped polymer stabilized fluorocarbon nanodroplets, which could be vaporized by FUS and/or laser pulses [147]. In this design, laser pulses are absorbed by the PPy component of the shell to induce a local temperature increase around the liquid core. They observed that when the nanodroplets were exposed to both optical and acoustic pulses, the threshold for photoacoustic signal generation decreased up to two orders of magnitude, which may be very useful in improving the contrast of deep tissue photoacoustic images (Figure 6). It should also be noted that super-resolution ultrasound imaging techniques developed by Tanter and coworkers makes it possible to detect single droplet vaporization events and may enable deep tissue photoacoustic or ultrasound imaging with ~10 μm resolution [148,149].

Several design parameters can affect the acoustic intensity threshold of phase-change droplet vaporization. Clearly, fluorocarbon selection is important. Depending on the boiling point of the selected materials, droplets can be evaporated at different acoustic pressures; using fluorocarbons with lower boiling points (higher vapor pressures) results in vaporization at lower acoustic intensities [150]. Another critical factor is the droplet size. Because the Laplace pressure across the spherical droplet interface decreases with increasing radius, larger droplets can be vaporized at lower acoustic pressures than smaller droplets [150]. The presence of large droplets in the droplet emulsion can cause background noise in the ultrasound (or photoacoustic images) since they can be evaporated at low acoustic intensities (or laser powers), so reducing the size dispersity of the droplet emulsions is important. On the other hand, if droplets require high acoustic pressures for evaporation, then mechanical damage at the imaged area may be observed. Therefore, the droplet vaporization threshold should be optimized concerning the

trade-off between acoustic activity and safety. It is important to note that the evaporation threshold not only depends on the acoustic pressure but also to the other acoustic parameters such as pulse duration, duty cycle, and pulse intensity. For instance, using longer FUS pulses, droplet vaporization can be achieved at lower acoustic pressures, but this can also cause a significant heat accumulation at the focal zone of FUS. Finally, there is a danger that superheated droplets, such as from DDFP, can fuse together and form gaseous emboli, so it is important for the interfacial stabilizing layer to be stable [151].

A recent study in our lab demonstrated that the composition of the stabilizing shell also has a profound effect on the vaporization threshold of the phase-change droplets (Figure 7A) [152]. Because of the short time scales (microseconds) for each pulse, the vaporization process follows nucleation and growth kinetics, in which each pulse provides a chance for creating critical vaporization nuclei in the droplet. It was found that mixtures of different lipids that exhibited lateral phase separation in the stabilizing lipid shell facilitated the ADV process. Therefore, at the same HIFU activation conditions, such droplets produced an order of magnitude higher ultrasound contrast than droplets with more isotropic shells. Our group also demonstrated that aggregated droplets could be vaporized at lower acoustic intensities as a means of detecting biomarkers acoustically (Figure 7B) [153]. In a proof of concept demonstration, streptavidin was detected at

concentrations down to 100 fM using biotin attached lipid stabilized PFH droplets with a mean radius of around 200 nm. Addition of streptavidin to such droplet emulsions results in aggregation of some droplets and decreases the acoustic vaporization threshold.

Phase change droplet formulations are also easily augmented with other molecules or moieties to expand capabilities beyond simple FUS sensitization. To impart targeting capabilities to phase-change droplets, the amphiphilic components comprising the shell can be functionalized with agents such as folic acid, peptides, or antibodies [31]. Superparamagnetic iron oxide nanoparticles (SPIONs) were added into the shells of droplets for magnetism-assisted targeting to the tumors [19,124,126]. In addition, SPIONs were served as MRI contrast agents to improve the contrast of MR images to provide better guidance to the HIFU therapy. Here, it should be noted that fluorocarbon cores of the phase-change droplets intrinsically serve as contrast agents for the ^{19}F -MR guidance of HIFU therapy [154]. However, ^{19}F MRI techniques are limited by the lack of clinical devices because most scanners are designed for ^1H -MRI [155]. Several other nanoparticles were also added to the fluorocarbon emulsions, including copper sulfide or gold nanorods as contrast agents for photoacoustic imaging [156,157], and bismuth sulfide as contrast agents for computed tomography and sensitizers for radiotherapy [18,158].

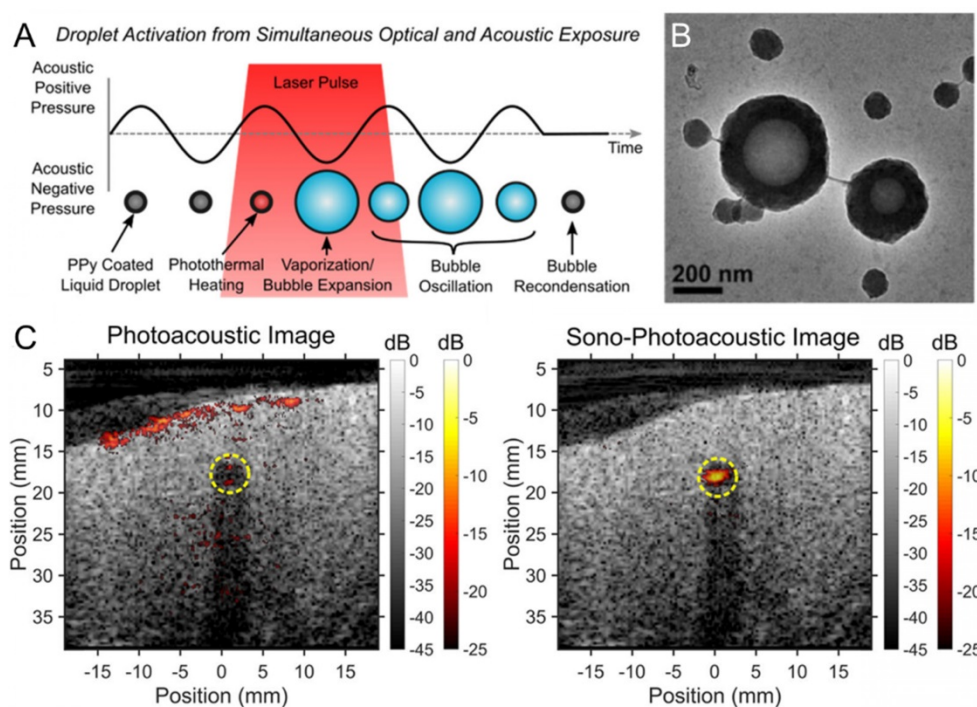


Figure 6. A) Schematic showing the nanodroplet vaporization using both optical and acoustic exposure. B) TEM image of the PPY coated droplets. C) Imaging of PPY coated droplets in chicken breast tissue; photoacoustic imaging (left) and sono-photoacoustic imaging (right). Adapted from reference [147], copyright 2016 American Chemical Society.

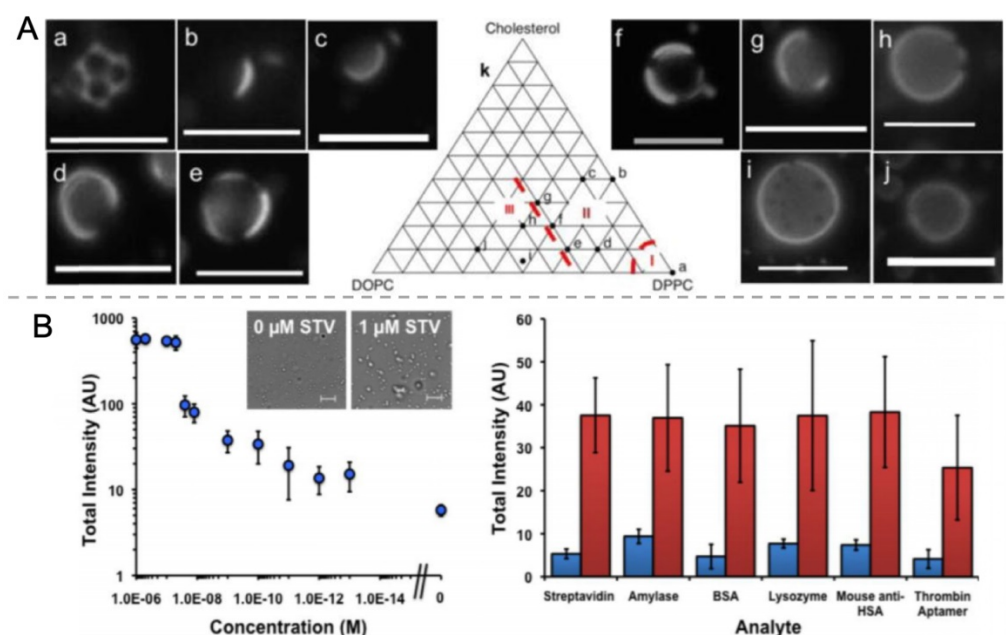


Figure 7. A) Fluorescence microscopy images of PFH droplets prepared using different mole percentages DPPC, DOPC, and Cholesterol. B) Schematic representation of nanodroplet aggregation and their activation by HIFU insonation (top) and ultrasound contrast generation as function of streptavidin concentration and in the presence of different analytes (bottom). Blue and red bars indicate ultrasound contrast without or with 1 nM streptavidin, respectively. A is reproduced from reference [152], copyright 2016 Royal Society of Chemistry. B is adapted from reference [153], copyright 2015 Wiley-VCH.

For drug delivery purposes, hydrophobic drugs can be easily loaded to fluorocarbon cores of the droplets. Various chemotherapy drugs such as doxorubicin, paclitaxel, methotrexate were loaded either to the phase-change droplets for tumor regression, prevention of metastasis, and elimination residual cancer cells survived after HIFU ablation [124,159–162]. While it is possible to load both hydrophobic and hydrophilic molecules to the stabilizing shells of the emulsions as with microbubbles, loading capacities are typically small [163,164]. To overcome this limitation, water-in-fluorocarbon-in-water double emulsions have been prepared in the expense of the significant increase in the particle size compared to regular phase-change droplets [25,165–167].

Because of their smaller size and capacity for extravasation, phase-change droplets have been applied towards imaging and treatment of solid tumors. For example, a manner similar to microbubbles, phase-change droplets have also been applied to create pores in tumor vasculature through inertial cavitation events to improve the accumulation of drugs or nanoparticles in solid tumors. Ho and Yeh observed significantly better penetration of liposomes into the tumor when they are co-administrated with phase-change droplets and treated with short FUS pulses to induce ADV [168]. In addition, a major challenge in cancer therapy is the presence of hypoxic regions in the tumor microenvironment, which causes resistance against several therapeutic approaches including chemotherapy and radiotherapy [169,170].

Due to their high oxygen-dissolving ability, fluorocarbon droplets are promising oxygen carriers for tumor reoxygenation [171,172]. FUS can be used to increase the oxygen release rate from droplets locally. Liu and coworkers were used to albumin-stabilized perfluoro-15-crown-5-ether nanodroplets for tumor oxygenation in 4T1 and CT-26 tumor models [173]. Instead of preloading the droplets with oxygen, they intravenously injected the droplets into tumor-bearing mice under hyperoxic breathing (Figure 8). Therefore, droplets adsorb oxygen in the lungs, and then the ones that reach to the tumor were treated with focused ultrasound to release their oxygen load. They showed that tumor oxygenation by using nanodroplets and FUS improved the outcomes of both radiotherapy and photodynamic tumor therapy in mice.

While phase-change droplets can be formulized in submicron sizes, they are not stable in practice when their sizes are smaller than 200 nm due to the high Laplace pressure. This particle size range is still larger than the optimal cutoff for the EPR effect [174,175]. Besides, there is also an intensive debate on the presence of EPR effect in human tumors to what extent, since nanoparticle delivery strategies that rely on EPR effect often fail in clinical trials [176]. Therefore, new strategies for delivering nanomaterials effectively to tumors is highly needed and currently under investigation. One such strategy is delivering nanomaterials using tumor-infiltrating cells, in which nanomaterials are first loaded into such cells *in vitro*, and then the loaded cells are intravenously injected

into the blood [177]. These 'cellular shuttles' then infiltrate into tumor tissue and deliver nanoparticles at the same time. Chiu et al. used this strategy to deliver an amphiphilic polymer stabilized perfluoropentane (PFP) nanodroplets by loading them into bone marrow-derived monocytes (Figure 9) [178]. They observed that nanodroplet loaded monocytes could penetrate to a depth beyond 150 μm away from the blood vessels, on the other hand, when just nanodroplets injected they could only penetrate up to a distance of 10-15 μm . While 80% of the free nanodroplets accumulated in the liver and only a small amount accumulated in the tumor, 60% of the nanodroplets were found in the tumor when they were administered within monocytes. Importantly, the nanodroplets remained acoustically active after loading them into the monocytes and produced significant ultrasound contrast in vivo after activation by FUS.

4.3. Fluorocarbon Infused Monodisperse Hollow Nanoparticles

While phase-change droplets have better stability than microbubbles, their stability is still not

sufficient for their long-term storage. This instability can be a major barrier to translation of phase-change droplets because they need to be prepared freshly with each administration, or used at most a few days after preparation. In addition, the inherent size dispersity of the as-prepared emulsions requires fractionation before use to eliminate the unwanted effects caused by easy cavitation of large droplets [153]. To overcome these limitations, researchers developed methods to load fluorocarbons to the hollow polymer or inorganic particles, usually monodisperse silica shells. For example, Kummel and coworkers, prepared silica shells with 500 nm diameters and loaded them with liquid PFP and used single HIFU pulse to initiate ADV process [183]. It was observed that when the surface of the shells was modified to target folate receptors, shells could generate contrast in vivo even after 12 days after administration. Such extended stability may be useful in long-term imaging of tumors, for instance, before and after surgical resection.

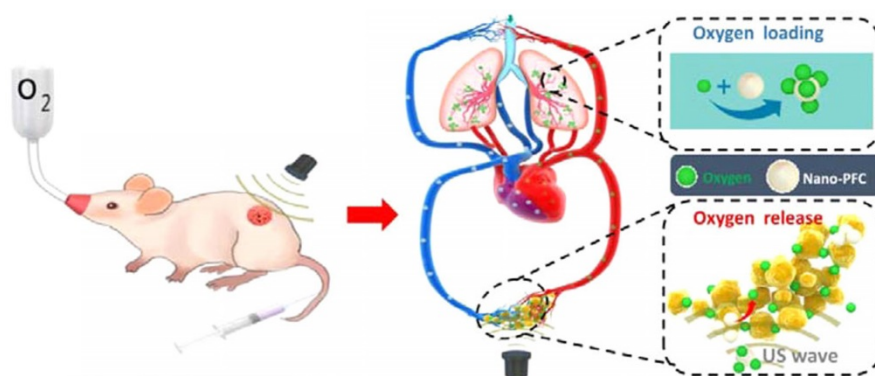


Figure 8. Ultrasound induced tumor oxygenation using phase-change droplets. Adapted from reference [173], copyright 2016 American Chemical Society.

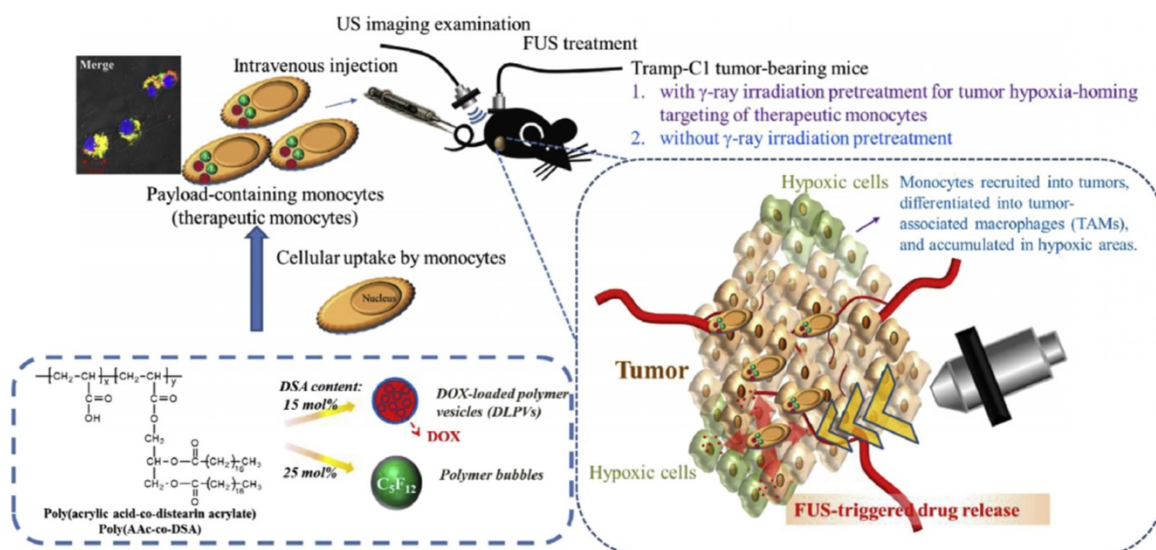


Figure 9. Schematic showing the delivery of phase-change droplets to tumors using monocytes. Adapted from reference [178], copyright 2015 Elsevier.

Shi and coworkers also developed several methods to prepare fluorocarbon loaded silica shells with sizes as small as ~ 100 nm and used HIFU to vaporize stabilized liquid in the hollow cores [174,179–182,184]. They observed larger ablated volumes both *ex vivo* and *in vivo* experiments when thermal HIFU was applied in the presence of fluorocarbon loaded silica shells. In addition, they used them to deliver chemotherapy drugs such as DOX. The same group also proposed to replace the fluorocarbons with low melting point molecules to improve the stability of the phase-change ultrasound active agents [185]. They used L-menthol, melts at ~ 45 °C, which is a temperature that can be easily attained by HIFU application. They showed that both hydrophobic and hydrophilic drug could be loaded into mesoporous silica shells, by simply mixing the shells, L-menthol, and drugs at elevated temperatures and then cooling to the room temperature. Upon HIFU insonation, the drug-loaded shells released their loaded due to the phase change of L-menthol. In a more recent study, they prepared isopentyl acetate, which has a boiling point of 142 °C, droplets coated with organosilica-iron oxide hybrid shells and demonstrated enhanced thermal HIFU ablation in a tumor-bearing mouse model [186].

4.4. Fluorocarbon-Free Colloidal Materials

Finally, another strategy to develop ultrasound-active materials with better *in vivo* stability and long shelf life is to eliminate the fluorocarbon fluid component entirely. It is well known that micro/nanoparticles with hydrophobic surfaces, cavities, or interfaces can act as nucleation sites for acoustic cavitation events and thus reduce the rarefactional acoustic pressures needed to generate acoustic cavitation [187–192]. An ultrasound imager can then detect the generated micron-sized bubbles during acoustic cavitation events as bright spots in the ultrasonograms [187]. Such contrast agents hold great promise in improving the lateral resolution of the molecular ultrasound imaging due to their smaller sizes and their better stability than common phase-change contrast agents. For example, Kwan et al. prepared divinylbenzene-crosslinked poly(methyl methacrylate) coated polystyrene nanocups, which can trap air pockets in their cavities to generate bubbles under reduced acoustic pressures [188]. High-speed camera imaging showed that the radius of the formed bubbles by nanocups ranged between a few tens of micrometers to over 100 μm depending on the acoustic parameters and the size of the nanocup cavity [193].

Our lab showed that amphiphilic (*e. g.* phospholipids, Pluronic polymers) stabilized hydrophobic MSNs with particle sizes ~ 100 nm can generate acoustically active microbubbles under reduced pressures of HIFU (Figure 10) [187,194]. Even though the coated hydrophobic MSNs were highly dispersible and stable in aqueous media, including PBS and serum, they can significantly reduce the acoustic cavitation threshold; down to ~ 6 MPa (peak negative pressure). Our studies suggested that such amphiphilic coated superhydrophobic MSNs stabilize air pockets (*i. e.* nanobubbles) at their surfaces, which are consumed for nucleation of micron-sized bubbles under reduced acoustic pressures [195]. We showed that the particles could be stored in PBS at least for four months or as lyophilized powders with no loss in contrast generation ability, indicating their stability to storage [187]. Under HIFU sonication, these particles can nucleate acoustic cavitation events continuously at low particle concentrations down to $\sim 2 \times 10^9$ particles mL^{-1} (*i. e.* ~ 5 $\mu\text{g mL}^{-1}$) for tens of minutes in several media including PBS, serum, whole blood, and tissue-mimicking phantoms [187]. In addition, it has been shown that they can remain acoustically active after being uptaken by cancer cells [194].

We also showed that the amphiphilic stabilized hydrophobic MSNs could locally enhance the mechanical effects of HIFU at relatively low acoustic pressures [194]. Ablation of red blood cells and tumor spheroids which are encapsulated in tissue-mimicking agarose phantoms was achieved at particle concentrations as low as 10 $\mu\text{g mL}^{-1}$, after HIFU treatment with a peak negative pressure of ~ 11 MPa and duty cycle of $\sim 0.01\%$ (20).

Such air stabilizing nanoparticles have been also showed to be useful in drug delivery applications (Figure 11). Coussios and coworkers showed that intravenously injected gas stabilizing nanocups could improve the intratumoral distribution of a freely circulating model therapeutic (IgG mouse antibody) when tumors were insonated with FUS [188]. Polymeric nanocups were also showed potential in improving delivery of nanoparticles into tumors [196]. To test this, microchannels were prepared using agarose gels, and nanocup and MSN dispersions were injected into the channels. The cavitation events generated by nanocups under FUS insonation, resulted in MSN penetration into the gels up to a distance of ~ 1 mm. Recently, they obtained similar results also using gas stabilizing gold nanocones [197]. Our group also showed that phospholipid stabilized hydrophobic MSNs can penetrate tissue mimicking gels up to a distance of 0.5 mm when exposed to HIFU [20].

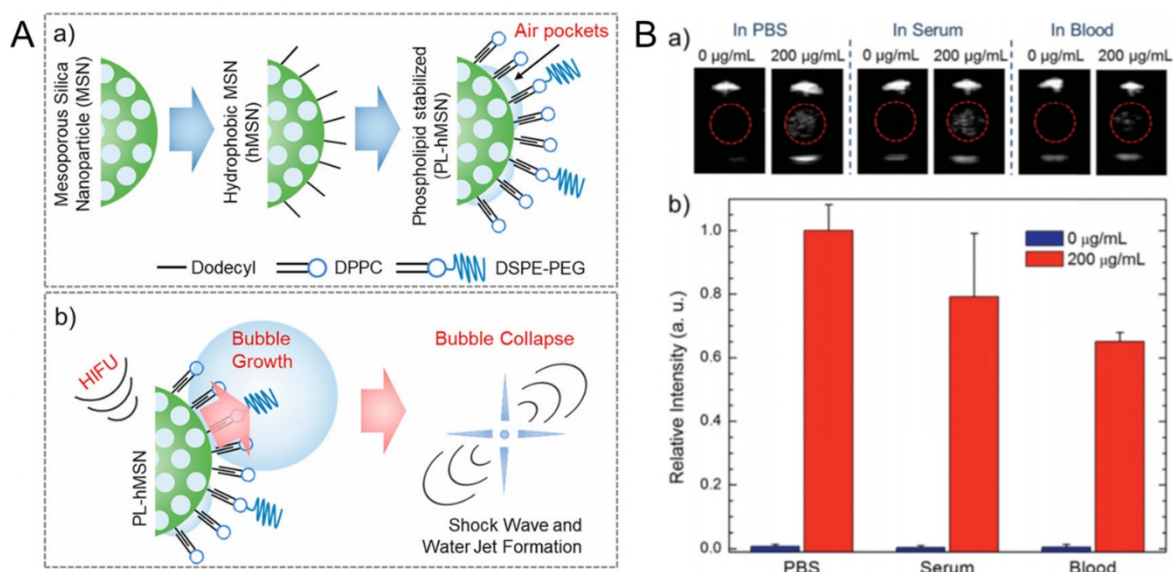


Figure 10. A) Schematics showing the preparation of phospholipid stabilized hydrophobic MSNs (a) and bubble generation by PL-hMSN under HIFU sonication (b). B) Ultrasound contrast generation by Pluronic polymer stabilized hydrophobic MSNs in different media. (a) Representative ultrasound images showing contrast generation during HIFU irradiation in the presence or absence of the Pluronic stabilized hydrophobic MSNs. (b) Relative contrast generation by the particles in different media. A is adapted from reference [20], copyright 2018 American Chemical Society. B is adapted from reference [187], copyright 2016 Wiley-VCH.

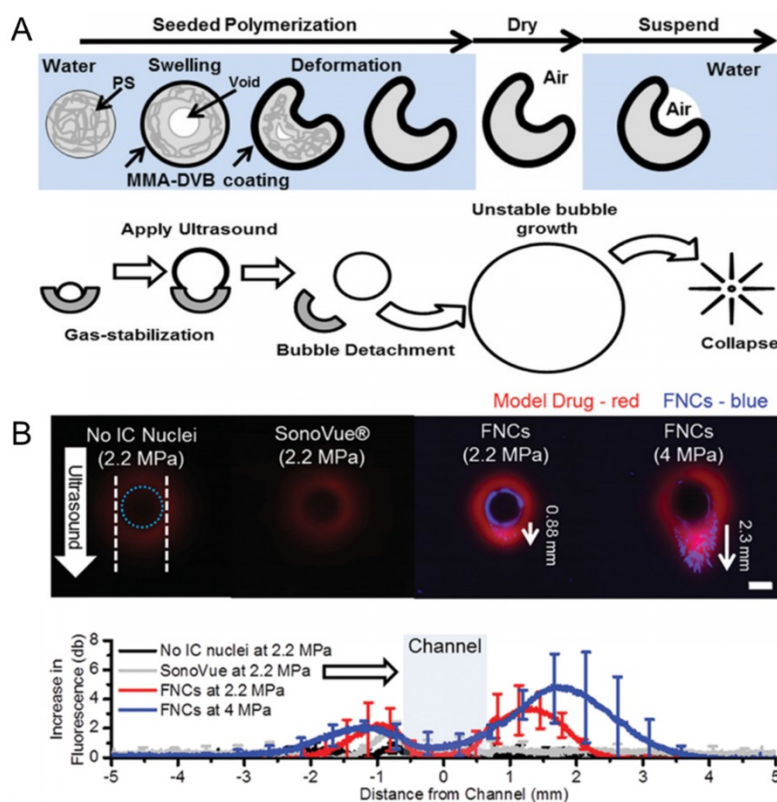


Figure 11. A) Schematic representation of polymeric nanocup preparation and bubble generation under ultrasound application. B) Penetration of nanocups and co-injected model drug into a tissue mimicking flow vessel after ultrasound exposure at different pressures for 5 min. Adapted from reference [188], copyright 2015 Wiley-VCH.

Regarding delivery of therapeutic molecules using the acoustic cavitation events by gas stabilizing nanoparticles (or any other kind of ultrasound active agent), one concern is the loss of therapeutic activity of these delicate molecules. For instance, mechanical and chemical effects induced by acoustic cavitation may denature or aggregate proteins or change the

molecular structures by breaking down the covalent bonds, reducing the double bonds and so on. Myers et al., studied the impact of cavitation events induced by gas stabilizing nanocups on the activity of a small molecule (doxorubicin, Dox), an antibody (cetuximab) and non-enveloped (adenovirus, Ad) and enveloped (VV) viral vectors [198]. They did not detect any

activity loss for any of the materials tested in *in vitro* conditions. Nevertheless, further studies are needed to fully evaluate the effects of cavitation on activity and structure of therapeutic molecules using different ultrasound parameters and *in vivo* models.

Beyond hydrophobic nanoparticles, some common hydrophilic nanoparticles such as gold nanoparticles and SPIONs have provided an increase in HIFU ablated volumes through a thermal mechanism. In one of such studies, Banerjee and coworkers applied commercially available 15 nm gold nanoparticles to improve the outcome of the thermal HIFU therapy (Figure 12A,B) [14]. They prepared tissue mimicking phantoms containing different amounts of gold nanoparticles and observed the temperature increase in phantoms using MR thermometry during HIFU treatment. In the presence of gold nanoparticles, higher temperature increase and larger lesion formation were observed at the same acoustic power compared to HIFU treatment in the absence of gold nanoparticles. A similar result has been previously observed by Wang et al., where they prepared PEGylated SPIONs to improve the contrast of the MR images to achieve better guidance for HIFU therapy [199]. They also observed that in the presence of SPIONs temperature increase in the tumor tissue was more than double compared to the sonication in the absence of SPIONs (15 °C vs. 38 °C). Józefczak and coworkers were obtained similar results in tissue-mimicking phantoms using SPIONs as well (Figure 12C) [200,201]. The improved temperature

increase in these studies is believed to be due to the enhanced attenuation and dissipation of acoustic energy in the presence of nanoparticles. Finally, the plasmon resonance has been leveraged for photoacoustic imaging. Such gold-silica core-shell nanoparticles are heated with a laser, they nucleate cavitation events and emit a photoacoustic response. Murray and coworkers showed that when gold nanoparticle containing tissue mimicking phantoms are subjected to both optical and ultrasound fields, a higher photoacoustic contrast can be obtained [202]. In addition, administration of FUS pulses reduced the laser power threshold for photoacoustic signal emission.

In recent years, gas generating nanoparticles have been designed to produce bubbles in the tumor microenvironment in response to the elevated temperature, low pH, or increased hydrogen peroxide concentration [203–206]. The bubble generation ability of such nanoparticles has also been applied to increase the volumes of HIFU ablated lesions. For example, Shi and coworkers prepared oxygen gas generating nanoparticles by loading catalase, an enzyme that degrades hydrogen peroxide to produce oxygen and water, into the pores of ~25 nm mesoporous silica nanoparticles with ~7 nm pores (Figure 13) [207]. They demonstrated the bubble generation at elevated H₂O₂ levels both *in vitro* and *in vivo* experiments and showed that these bubbles could increase the thermal HIFU ablated volumes. Wang and coworkers, on the other hand, prepared ammonium bicarbonate loaded

liposomes, which produce CO₂ bubbles at elevated temperatures, and used HIFU to locally increase the temperatures to initiate bubble generation by the liposomes [208]. Similarly, larger ablated volumes were obtained in the presence of bubble-generating liposomes. Nanoparticles can also be designed to the on-demand release of therapeutic gases such as toxic nitric oxide under FUS insonation. Chen and coworkers prepared hollow MSNs and decorated their surfaces with L-arginine as a natural nitric oxide generator, which reacts with H₂O₂ to generate nitric oxide [209]. They showed that application of FUS catalyzes this reaction and enhanced the

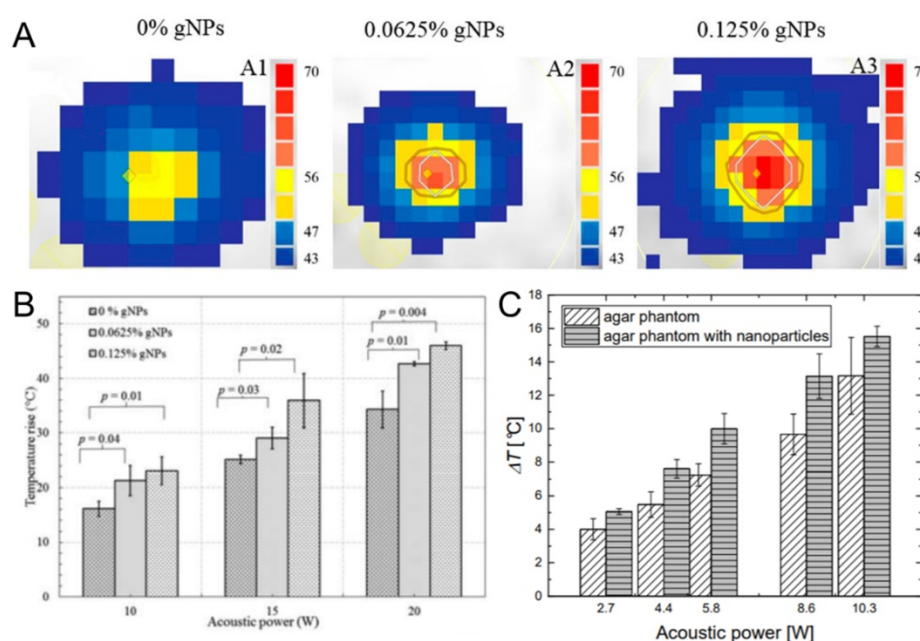


Figure 12. A) Temperature maps of tissue-mimicking phantoms containing different amounts of gold nanoparticles after treated with HIFU at 10 W. B) Maximum temperature rise in tissue mimicking phantoms containing different amounts of gold nanoparticles after HIFU insonation at different acoustic powers. C) Temperature increase in tissue mimicking phantoms containing or not containing iron oxide nanoparticles after HIFU treatment at different acoustic powers. A and B are adapted from reference [14], copyright 2017 American Chemical Society. C is adapted from reference [201], copyright 2018 MDPI.

nitric oxide production by the nanoparticles and increased the survival rate of mice with Panc-1 pancreatic tumors.

While these fluorocarbon-free nanomaterials are promising for the development of robust and smaller agents for FUS theranostics, extensive research must be performed prior to clinical adaptation to evaluate several performance and safety-related issues such as biocompatibility, biodegradation, tumor accumulation, and stability in vivo. This is also the case for the fluorocarbon loaded inorganic or polymer shells described in previous sections. Another challenge for successful translation of nanomaterials to clinic is the lack of scalable, cost-effective, and reproducible methods for their synthesis.

4.5. Stimuli-Responsive Colloidal Materials

The use of stimuli-responsive colloids in FUS research has been mainly in ultrasound triggered drug delivery by both thermal and mechanical effects. Among the stimuli-responsive materials, the most studied ones in this area are the temperature sensitive liposomes, which can release their loads at mild-hyperthermia conditions that are locally achieved by FUS insonation [210–212]. For example, Dromi et al. used a commercially available low-temperature sensitive liposome formulation

(ThermoDox, Celsion Corp.), which changes its structure when heated to around 40–45 °C to release encapsulated DOX [211]. They also used another commercially available but not temperature responsive DOX liposome formulation (Doxil, Ortho Biotech Products) for control experiments. When they sonicated the liposomes in vitro to increase the temperature around 42 °C, they observed that 50% of DOX released from ThermoDox, but there was not any detectable from Doxil. In a mouse tumor model, they observed a significantly better tumor growth reduction compared to free DOX and Doxil liposomes for ThermoDox which is activated by HIFU application. However, low temperature responsive liposomes have poor morphological stability in the bloodstream which may cause the off-target release of the loaded drug. To improve structural stability and minimize drug leakage during blood circulation, Liang et al. developed a method to create crosslinks in the lipid bilayer using a sol-gel reaction [213]. As a result, an increased blood circulation half-life was observed for crosslinked temperature responsive liposomes compared to the conventional ones, from 0.9 to 8.5 h.

Other studies reported drug release from liposomes or micelles due to mechanical forces such as shear forces, microstreaming, and water jet

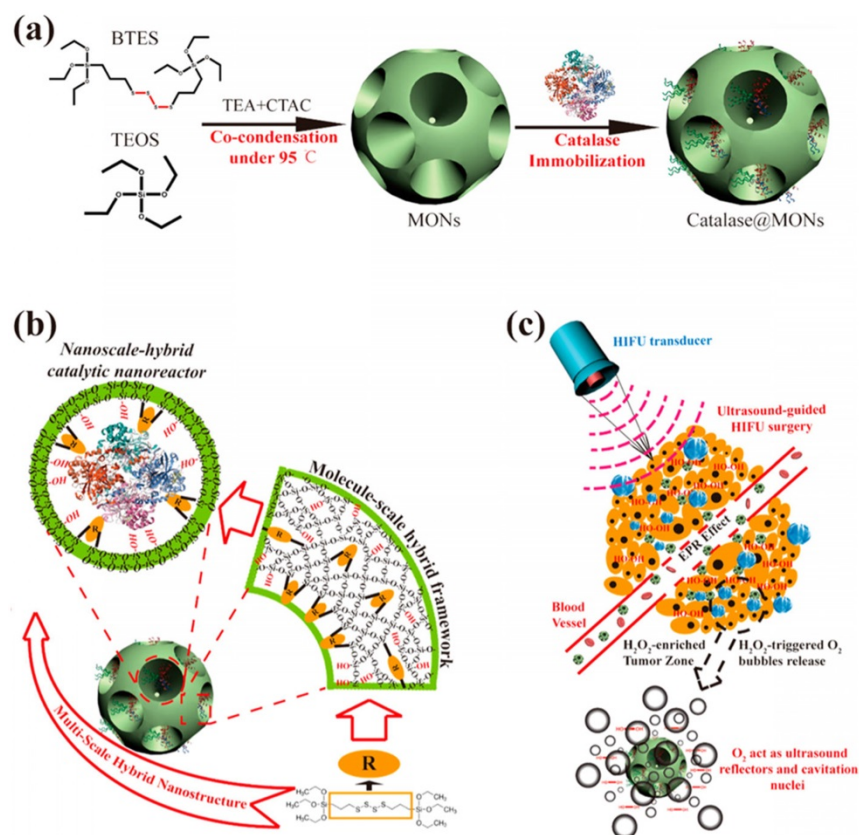


Figure 13. Schematic representation of the preparation of catalase loaded large pore mesoporous silica nanoparticles and improved HIFU therapy in the presence of bubbles generated by the catalytic particles. Reproduced from reference [207], copyright 2017 American Chemical Society.

formation [214,215]. As discussed in Section 3, the selection of the FUS parameters determines either thermal or mechanical effects will be more predominant. This is especially important for temperature responsive materials, and to our knowledge, there is not any study that investigates the contribution of mechanical effects on the drug release from temperature responsive liposomes or micelles. Clearly, further studies are needed to fully understand the FUS-triggered drug release from micelles and liposomes that are temperature responsive or not.

Another strategy for temperature-responsive drug carriers are porous drug carriers coated with temperature-sensitive polymers. At low temperatures, the polymer chains around the drug carriers are tightly packed and thus block the pores of these carriers and prevent or limit the drug release. At elevated temperatures, such polymers can shrink, or the interactions between different polymer chain can be weakened. In either case, the pores become less blocked, and drugs can be released. For this purpose, Li et al. used gold nanocages coated with a temperature responsive copolymer, poly(NIPAAm-co-AAm) (NIPAAm: N-isopropylacrylamide; AAm: acrylamide), and showed that upon HIFU insonation the gold nanocages released a model drug (Rhodamine 6G) due to the shrinkage of pore blocking copolymer at elevated temperatures [216].

The application of FUS can also induce chemical changes (*i.e.*, bond breakage or reorganization) in stimuli-responsive polymers. For example, Wang et al. showed that poly(ethylene oxide) and poly(2-tetrahydropyranyl methacrylate) diblock copolymer micelles could be disrupted by HIFU insonation due to the hydrolysis of side chains of 2-tetrahydropyranyl methacrylate block [217]. The hydrolytic cleavage of a relatively more hydrophobic group makes the polymer more hydrophilic and, thus, disturb the micelle structure, which eventually increases the rate of drug release from the micelles. Tong et al., on the other hand, prepared redox-responsive amphiphilic copolymers by adding disulfide bond between the hydrophobic and hydrophilic groups [218]. They observed that the release rate from the redox-responsive micelles was especially improved under HIFU sonication in the presence of a redox agent, dithiothreitol, due to the cleavage of disulfide bonds.

4.6. Acoustically Active Hydrogels and Membranes

Acoustically active hydrogels or membranes have also been designed primarily for FUS induced on-demand drug delivery. A straightforward strategy

is loading drug-laden temperature responsive liposomes into hydrogels and locally heating them above their phase transition temperatures using appropriate FUS parameters to trigger drug release from the hydrogels [219]. For example, Ruiz-Hernández and coworkers were encapsulated DOX-loaded temperature responsive liposomes in an injectable chitosan/ β -glycerophosphate hydrogel and showed the on-demand release of DOX at elevated temperatures ($\sim 42^\circ\text{C}$), which could be easily achieved by FUS insonation [220].

In addition to the heating effect of FUS, mechanical effects generated by ultrasound active agents can be applied to control the release from hydrogels. In this context, microbubble or phase-change droplet loaded hydrogels have been applied to locally deliver therapeutics such as drugs, growth factors, micro/nanoparticles. For instance, Fabiilli and coworkers have developed several fibrin hydrogel scaffolds for growth factor delivery, such fibroblast growth factor (bFGF), by loading microbubbles or nanodroplet and growth factor into scaffolds [221–224]. Wang and coworkers, on the other hand, have used membranes with $12\ \mu\text{m}$ conical pores and they loaded these pores with silica particles and phase-change droplets [225]. They showed that vaporization of phase-change droplets using FUS fired the silica nanoparticles from these “microcannons,” which could be useful for transdermal delivery (Figure 14) [226]. Later they also used this strategy for transdermal delivery of an anesthetic agent lidocaine [227]. However, metastability of these fluorocarbon-based ultrasound active agents prevents their long-term use as they evaporate or dissolve in hydrogels in a few days, and thus, hydrogels lose their ultrasound activity [223,224].

To develop a more robust on-demand drug delivery system, Grinstaff and coworkers used drug-loaded superhydrophobic meshes, which entrap air layers and thus prevent both water penetration and drug release [228]. The authors found that when they treated the superhydrophobic meshes with HIFU, water could locally infiltrate to trigger the drug release. They also showed that this approach could be used to kill cancer cells *in vitro* after HIFU administration through the release of a chemotherapeutic drug. In a similar approach, Wang et al. prepared hydrophobic PLGA gels, which again prevents water penetration inside the gels [229]. After locally degrading the air barrier between the water and the gel using HIFU, water penetrates the gel, where it reacts with the pre-loaded sodium bicarbonate to produce CO_2 bubbles. Finally, they showed that the release of DOX molecules

encapsulated in the hydrophobic gels, accelerated by the generated bubbles.

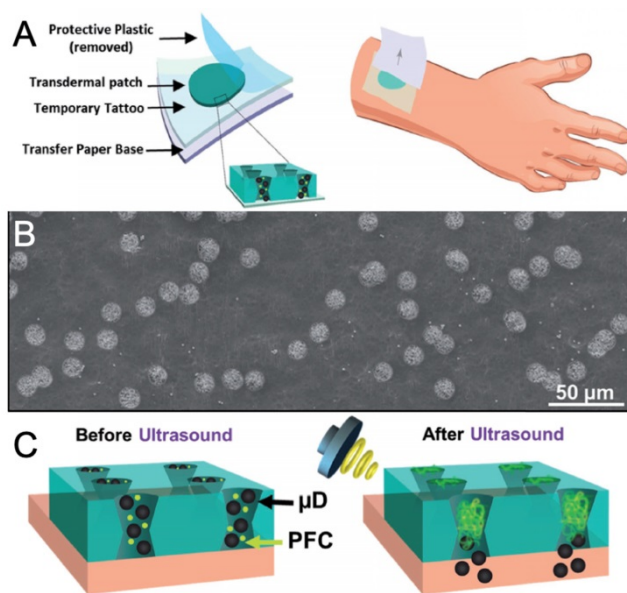


Figure 14. A) Schematic showing the tattoo patch. B) SEM image of the tattoo patch. C) Schematic showing drug delivery by vaporization of fluorocarbon droplets. Adapted from reference [226] copyright 2017 Wiley-VCH.

Gai et al., also used trapped air inside the microwells for the on-demand release of encapsulated drugs [230]. They first prepared microwells on PDMS membranes and loaded the wells with a model compound; Rhodamine B. Then, they sealed the wells using a hydrophobic polymer, polylactic acid. During the sealing step, air pockets were also encapsulated in the wells. These air pockets have two essential functions: 1) they prevent the release of the loaded molecules for 14 days under submerged conditions in the absence of HIFU activation and 2) nucleates acoustic cavitation events inside the wells under HIFU insonation, which breaks the polymer caps of the wells and the loaded drugs are released.

5. Future Directions and Challenges

FUS has shown success in the non-invasive treatment of several diseases, including cancer, neurodegenerative diseases, and thrombolysis. However, the high acoustic reflection and scattering at interfaces of soft tissue with gas and bone makes it challenging to apply FUS to some parts of the body such as ribs, lungs, and cranium. In addition, the unwanted scattering of ultrasound at such interfaces may cause off-target damage. Application of materials capable of interacting with ultrasound can increase the local mechanical and thermal effects of FUS while simultaneously reducing the FUS intensities required to initiate cavitation. By optimizing the properties of these materials, theranostic efficacy could be

improved and unwanted off-target damage minimized.

One of the main challenges is delivering the ultrasound active agents to the intended tissue, as most agents have large sizes and poor stability in the bloodstream that prevent their extravasation from the vasculature. To bypass issues with stability, fluorocarbon-free robust ultrasound active materials have been synthesized sizes smaller than 200 nm, which can potentially extravasate from the blood circulation and accumulate better in target tissue [188,194,207,231]. However, smaller particle size and better stability do not always guarantee improved accumulation of nanoparticles in the target tissue, especially for solid tumors. We now know that the EPR effect, which only counts the number and size of the openings in the tumor vasculature, is an oversimplified model for predicting the nanoparticle accumulation and penetration in tumors [232–234]. First, it does not take into account immune surveillance during circulation. Second, while the vasculature in fast-growing xenograft mice tumors usually possess considerable leakiness, this is not always the case for slow-growing human tumors with fewer openings in the vasculature due to their lower growth rate. Tumor leakiness not only varies with tumor type but also from patient to patient. Furthermore, in the tumor microenvironment, there are several other barriers such as high interstitial fluid pressure, thick tumor stroma, macrophage uptake that prevent deep tumor penetration and uniform accumulation of nanoparticles and their uptake by cancer cells [232,235–237]. Thus, the mechanical damage induced by FUS-sensitizing particles represent an opportunity to create pores in the tumor vasculature and stroma. For example, a FUS active material could first be administered to porate the tumor, followed by repeated administration of a therapeutic agent. Thus, the recent advances in the ultrasound active agent design such fluorocarbon-free robust nanoparticles may provide more opportunities to the researchers to optimize the physical and chemical properties of the materials to reach the desired acoustic activity, target tissue accumulation and biosafety.

In terms of the FUS itself, another problem is the inadequate reporting of acoustic parameters used in the studies. While in principle the experimental methods section should contain sufficient detail to reproduce insonation conditions, in practice FUS parameters are often inconsistently characterized or even incomplete. At a minimum, the operating frequency of the transducer, the pulse duration (and the number of cycles), pulse-repetition frequency (or duty cycle), and the peak positive and negative

pressure amplitudes (and corresponding intensities) of the resulting waveform should be given in order to reproduce any given work. As discussed above each of these parameters can have a significant impact on the type and efficacy of the predominant effect generated by the FUS application. Unfortunately, reports of only the applied wattage or output acoustic intensity are common, which are insufficient for determining the experimental conditions used in such studies. Therefore, there is a need to establish a “minimum information standard,” as has been established in the greater nanomedicine field to provide better reproducibility to the published works and allow to comparison of experimental parameters used across different works [238,239].

In conclusion, the last several years have seen many exciting developments in the acoustically active material design. Such materials not only helped to improve the outcomes from the conventional HIFU ablation therapy and using FUS for BBBO but have also opened new avenues in drug delivery, bioimaging, and others. However, prior to their clinical translation, there are several issues still needs to be addressed such as sufficient accumulation in the target tissue, biocompatibility, clearance from the body, large-scale production, and storage stability. Finally, there is an urgent need to develop minimum information reporting standards to enhance reproducibility and comparability in the field.

Competing Interests

The authors have declared that no competing interest exists.

References

- Kennedy JE. High-intensity focused ultrasound in the treatment of solid tumours. *Nat Rev Cancer*. 2005; 5: 321–7.
- Maliotzis G, Monzon L, Hand J, Wasan H, Leen E, Abel M, et al. High-intensity focused ultrasound: advances in technology and experimental trials support enhanced utility of focused ultrasound surgery in oncology. *Br J Radiol*. 2013; 86: 20130044.
- Mitragotri S. Healing sound: the use of ultrasound in drug delivery and other therapeutic applications. *Nat Rev Drug Discov*. 2005; 4: 255–60.
- Parsons JE, Cain CA, Abrams GD, Fowlkes JB. Pulsed cavitation ultrasound therapy for controlled tissue homogenization. *Ultrasound Med Biol*. 2006; 32: 115–29.
- Haar GRT. High intensity focused ultrasound for the treatment of tumors. *Echocardiography*. 2001; 18: 317–22.
- Tempamy CMC, McDannold NJ, Hynynen K, Jolesz FA. Focused ultrasound surgery in oncology: Overview and principles. *Radiology*. 2011; 259: 39–56.
- Al-Bataineh O, Jenne J, Huber P. Clinical and future applications of high intensity focused ultrasound in cancer. *Cancer Treat Rev*. 2012; 38: 346–53.
- Hsiao Y-H, Kuo S-J, Tsai H-D, Chou M-C, Yeh G-P. Clinical application of high-intensity focused ultrasound in cancer therapy. *J Cancer*. 2016; 7: 225–31.
- Chu KF, Dupuy DE. Thermal ablation of tumours: Biological mechanisms and advances in therapy. *Nat Rev Cancer*. 2014; 14: 199–208.
- Roberts WW, Hall TL, Ives K, Wolf JS, Fowlkes JB, Cain CA. Pulsed cavitation ultrasound: a noninvasive technology for controlled tissue ablation (histotripsy) in the rabbit kidney. *J Urol*. 2006; 175: 734–8.
- Hall TL, Hempel CR, Wojno K, Xu Z, Cain CA, Roberts WW. Histotripsy of the prostate: dose effects in a chronic canine model. *Urology*. 2009; 74: 932–7.
- Timbie KF, Mead BP, Price RJ. Drug and gene delivery across the blood-brain barrier with focused ultrasound. *J Control Release*. 2015; 219: 61–75.
- Hijnen N, Kneepkens E, de Smet M, Langereis S, Heijman E, Grüll H. Thermal combination therapies for local drug delivery by magnetic resonance-guided

- high-intensity focused ultrasound. *Proc Natl Acad Sci USA*. 2017; 114: E4802–11.
- Devarakonda SB, Myers MR, Lanier M, Dumoulin C, Banerjee RK. Assessment of gold nanoparticle-mediated-enhanced hyperthermia using mr-guided high-intensity focused ultrasound ablation procedure. *Nano Lett*. 2017; 17: 2532–8.
- Cirincione R, Di Maggio FM, Forte GI, Minafra L, Bravata V, Castiglia L, et al. High-intensity focused ultrasound- and radiation therapy-induced immuno-modulation: comparison and potential opportunities. *Ultrasound Med Biol*. 2017; 43: 398–411.
- Liberman A, Wu Z, Barback CV, Viveros RD, Wang J, Ellies LG, et al. Hollow iron-silica nanoshells for enhanced high intensity focused ultrasound. *J Surg Res*. 2014; 190: 391–8.
- Zhou Y, Wang Z, Chen Y, Shen H, Luo Z, Li A, et al. Microbubbles from gas-generating perfluorohexane nanoemulsions for targeted temperature-sensitive ultrasonography and synergistic HIFU ablation of tumors. *Adv Mater*. 2013; 25 4123–30.
- Yao M, Ma M, Chen Y, Jia X, Xu G, Xu H, et al. Multifunctional Bi2S3/PLGA nanocapsule for combined HIFU/radiation therapy. *Biomaterials*. 2014; 35(28): 8197–205.
- Sun Y, Zheng Y, Ran H, Zhou Y, Shen H, Chen Y, et al. Superparamagnetic PLGA-iron oxide microcapsules for dual-modality US/MR imaging and high intensity focused US breast cancer ablation. *Biomaterials*. 2012; 33: 5854–64.
- Yildirim A, Shi D, Roy S, Blum NT, Chattaraj R, Cha JN, et al. Nanoparticle-mediated acoustic cavitation enables high intensity focused ultrasound ablation without tissue heating. *ACS Appl Mater Interfaces*. 2018; 10: 36786–95.
- Yoon YI, Tang W, Chen X. Ultrasound-mediated diagnosis and therapy based on ultrasound contrast agents. *Small Methods*. 2017; 1: 1700173.
- Chen Y, Chen H, Shi J. Nanobiotechnology promotes noninvasive high-intensity focused ultrasound cancer surgery. *Adv Healthc Mater*. 2015; 4: 158–65.
- Qian X, Han X, Chen Y. Insights into the unique functionality of inorganic micro/nanoparticles for versatile ultrasound theranostics. *Biomaterials*. 2017; 142: 13–30.
- Misra SK, Ghoshal G, Gartia MR, Wu Z, De AK, Ye M, et al. Trimodal therapy: Combining hyperthermia with repurposed Bezarotene and ultrasound for treating liver cancer. *ACS Nano*. 2015; 9: 10695–718.
- Juliar BA, Bromley MM, Moncion A, Jones DC, O'Neill EG, Wilson CG, et al. In situ transfection by controlled release of lipoplexes using acoustic droplet vaporization. *Adv Healthc Mater*. 2016; 5: 1764–74.
- Airan RD, Meyer RA, Ellens NPK, Rhodes KR, Farahani K, Pomper MG, et al. Noninvasive targeted transcranial neuromodulation via focused ultrasound gated drug release from nanoemulsions. *Nano Lett*. 2017; 17: 652–9.
- Hsieh C-C, Kang S-T, Lin Y-H, Ho Y-J, Wang C-H, Yeh C-K, et al. Biomimetic acoustically-responsive vesicles for theranostic applications. *Theranostics*. 2015; 5: 1264–74.
- Zhou Y, Han X, Jing X, Chen Y. Construction of silica-based micro/nanoplatfoms for ultrasound theranostic biomedicine. *Adv Healthc Mater*. 2017; 6: 1700646.
- Tang H, Zheng Y, Chen Y. Materials chemistry of nanoultrasonic biomedicine. *Adv Mater*. 2017; 29: 1604105.
- Sirsi SR, Borden MA. State-of-the-art materials for ultrasound-triggered drug delivery. *Adv Drug Deliv Rev*. 2014; 72: 3–14.
- Son S, Min HS, You DG, Kim BS, Kwon IC. Echogenic nanoparticles for ultrasound technologies: Evolution from diagnostic imaging modality to multimodal theranostic agent. *Nano Today*. 2014; 9: 525–40.
- Curie J, Curie P. Développement par compression de l'électricité polaire dans les cristaux hémiedres à faces inclinées. *Bull Minéral*. 1880; 3: 90–3.
- Curie J, Curie P. Contractions and expansions produced by voltages in hemihedral crystals with inclined faces. *Comptes Rendus*. 1881; 93: 1137–40.
- Newman PG, Rozycki GS. The history of ultrasound. *Surgical Clinics*. 1998; 78: 179–95.
- Wood RW, Loomis AL. The physical and biological effects of high-frequency sound-waves of great intensity. *Phil Mag*. 1927; 4: 417–36.
- Gruetzmacher J. Piezoelektrischer Kristall mit Ultrashallkonvergenz. *Z Physik*. 1935; 96: 342–9.
- Lynn JG, Zwemer RL, Chick AJ, Miller AE. A new method for the generation and use of focused ultrasound in experimental biology. *J Gen Physiol*. 1942; 26: 179–93.
- Fry WJ, Barnard JW, Fry EJ, Krumins RF, Brennan JF. Ultrasonic lesions in the mammalian central nervous system. *Science*. 1955; 122: 517–8.
- Haar GT, Coussios C. High intensity focused ultrasound: physical principles and devices. *Int J Hyperthermia*. 2007; 23: 89–104.
- Dubinsky TJ, Cuevas C, Dighe MK, Kolokythas O, Hwang JH. High-intensity focused ultrasound: current potential and oncologic applications. *AJR Am J Roentgenol*. 2008 Jan; 190: 191–9.
- Jolesz FA. MRI-guided focused ultrasound surgery. *Annu Rev Med*. 2009; 60: 417–30.
- Leighton TG. What is ultrasound? *Prog Biophys Mol Biol*. 2007; 93: 3–83.
- Hayes BT, Merrick MA, Sandrey MA, Cordova ML. Three-MHz ultrasound heats deeper into the tissues than originally theorized. *J Athl Train*. 2004; 39: 230–4.

44. Bailey MR, Khokhlova VA, Sapozhnikov OA, Kargl SG, Crum LA. Physical mechanisms of the therapeutic effect of ultrasound (a review). *Acoust Phys*. 2003; 49: 369–88.
45. Parsons JE, Cain CA, Fowlkes JB. Cost-effective assembly of a basic fiber-optic hydrophone for measurement of high-amplitude therapeutic ultrasound fields. *J Acoust Soc Am*. 2006; 119: 1432–40.
46. Zhou Y, Zhai L, Simmons R, Zhong P. Measurement of high intensity focused ultrasound fields by a fiber optic probe hydrophone. *J Acoust Soc Am*. 2006; 120: 676–85.
47. Preston RC. Output measurements for medical ultrasound. Berlin, Germany: Springer-Verlag; 1991
48. Suslick KS, Eddingsaas NC, Flannigan DJ, Hopkins SD, Xu H. The chemical history of a bubble. *Acc Chem Res*. 2018; 51: 2169–78.
49. Muratore R. A History of the Sonicare CST-100: The First FDA-approved HIFU device. AIP Conference Proceedings. Boston, Massachusetts (USA): AIP; 2006
50. Illing RO, Kennedy JE, Wu F, ter Haar GR, Protheroe AS, Friend PJ, et al. The safety and feasibility of extracorporeal high-intensity focused ultrasound (HIFU) for the treatment of liver and kidney tumours in a Western population. *Br J Cancer*. 2005; 93: 890–5.
51. Golan R, Bernstein A, Sedrakyan A, Daskivich TJ, Du DT, Ehdia B, et al. Development of a nationally representative coordinated registry network for prostate ablation technologies. *J Urol*. 2018; 199: 1488–93.
52. Khokhlova VA, Fowlkes JB, Roberts WW, Schade GR, Xu Z, Khokhlova TD, et al. Histotripsy methods in mechanical disintegration of tissue: towards clinical applications. *Int J Hyperthermia*. 2015; 31: 145–62.
53. Hoogenboom M, Eikelenboom D, den Brok MH, Heerschap A, Fütterer JJ, Adema GJ. Mechanical high-intensity focused ultrasound destruction of soft tissue: working mechanisms and physiologic effects. *Ultrasound Med Biol*. 2015; 41: 1500–17.
54. Peek MCL, Wu F. High-intensity focused ultrasound in the treatment of breast tumours. *Ecanermedicalscience*. 2018; 12: 794.
55. Khokhlova TD, Wang Y-N, Simon JC, Cunitz BW, Starr F, Paun M, et al. Ultrasound-guided tissue fractionation by high intensity focused ultrasound in an in vivo porcine liver model. *Proc Natl Acad Sci USA*. 2014; 111: 8161–6.
56. Khokhlova TD, Monsky WL, Haider YA, Maxwell AD, Wang Y-N, Matula TJ. Histotripsy liquefaction of large hematomas. *Ultrasound Med Biol*. 2016; 42: 1491–8.
57. Vlaisavljevich E, Durmaz YY, Maxwell A, Elsayed M, Xu Z. Nanodroplet-mediated histotripsy for image-guided targeted ultrasound cell ablation. *Theranostics*. 2013; 3: 851–64.
58. Kieran K, Hall TL, Parsons JE, Wolf JS, Fowlkes JB, Cain CA, et al. Refining histotripsy: defining the parameter space for the creation of nonthermal lesions with high intensity, pulsed focused ultrasound of the in vitro kidney. *J Urol*. 2007; 178: 672–6.
59. Qian X, Zheng Y, Chen Y. Micro/nanoparticle-augmented sonodynamic therapy (sdT): breaking the depth shallow of photoactivation. *Adv Mater*. 2016; 28: 8097–129.
60. Kripfgans OD, Zhang M, Fabiilli ML, Carson PL, Padilla F, Swanson SD, et al. Acceleration of ultrasound thermal therapy by patterned acoustic droplet vaporization. *J Acoust Soc Am*. 2014; 135: 537–44.
61. Song K-H, Harvey BK, Borden MA. State-of-the-art of microbubble-assisted blood-brain barrier disruption. *Theranostics*. 2018; 8: 4393–408.
62. Chang N, Lu S, Qin D, Xu T, Han M, Wang S, et al. Efficient and controllable thermal ablation induced by short-pulsed HIFU sequence assisted with perfluorohexane nanodroplets. *Ultrasound Sonochem*. 2018; 45: 57–64.
63. Chen CC, Sheeran PS, Wu S-Y, Olumolade OO, Dayton PA, Konofagou EE. Targeted drug delivery with focused ultrasound-induced blood-brain barrier opening using acoustically-activated nanodroplets. *J Control Release*. 2013; 172: 795–804.
64. Pardridge WM. Blood-brain barrier drug targeting: the future of brain drug development. *Mol Interv*. 2003; 3: 90.
65. Pardridge WM. The blood-brain barrier: bottleneck in brain drug development. *NeuroRx*. 2005; 2: 3–14.
66. Vykhotseva N, McDannold N, Hynynen K. Progress and problems in the application of focused ultrasound for blood-brain barrier disruption. *Ultrasonics*. 2008; 48: 279–96.
67. Barnard JW, Fry WJ, Fry FJ, Krumins RF. Effects of high intensity ultrasound on the central nervous system of the cat. *J Comp Neuro*. 1955; 103: 459–84.
68. Vykhotseva NI, Hynynen K, Damianou C. Histologic effects of high intensity pulsed ultrasound exposure with subharmonic emission in rabbit brain in vivo. *Ultrasound Med Biol*. 1995; 21: 969–79.
69. Hynynen K, McDannold N, Vykhotseva N, Jolesz FA. Noninvasive MR imaging-guided focal opening of the blood-brain barrier in rabbits. *Radiology*. 2001; 220: 640–6.
70. Vykhotseva N, Sorrentino V, Jolesz FA, Bronson RT, Hynynen K. MRI detection of the thermal effects of focused ultrasound on the brain. *Ultrasound Med Biol*. 2000; 26: 871–80.
71. Correias JM, Bridal L, Lesavre A, Méjean A, Claudon M, Hélénon O. Ultrasound contrast agents: properties, principles of action, tolerance, and artifacts. *Eur Radiol*. 2001; 11: 1316–28.
72. Miller DL, Averkiou MA, Brayman AA, Everbach EC, Holland CK, Wible JH, et al. Bioeffects considerations for diagnostic ultrasound contrast agents. *J Ultrasound Med*. 2008; 27: 611–32.
73. Schutt EG, Klein DH, Mattrey RM, Riess JG. Injectable microbubbles as contrast agents for diagnostic ultrasound imaging: the key role of perfluorochemicals. *Angew Chem Int Ed*. 2003; 42: 3218–35.
74. Stride E, Saffari N. Microbubble ultrasound contrast agents: a review. *Proc Inst Mech Eng H*. 2003; 217: 429–47.
75. Ferrara K, Pollard R, Borden M. Ultrasound microbubble contrast agents: fundamentals and application to gene and drug delivery. *Annu Rev Biomed Eng*. 2007; 9: 415–47.
76. Unger EC, Porter T, Culp W, Labell R, Matsunaga T, Zutshi R. Therapeutic applications of lipid-coated microbubbles. *Adv Drug Deliv Rev*. 2004; 56: 1291–314.
77. Yu T, Wang G, Hu K, Ma P, Bai J, Wang Z. A microbubble agent improves the therapeutic efficiency of high intensity focused ultrasound: a rabbit kidney study. *Urol Res*. 2004; 32: 14–9.
78. Yu T, Xiong S, Mason TJ, Wang Z. The use of a micro-bubble agent to enhance rabbit liver destruction using high intensity focused ultrasound. *Ultrasound Sonochem*. 2006; 13: 143–9.
79. Xu RX, Povoski SP, Martin EW. Targeted delivery of microbubbles and nanobubbles for image-guided thermal ablation therapy of tumors. *Expert Rev Med Devices*. 2010; 7: 303–6.
80. McDannold N, Zhang Y, Vykhotseva N. Nonthermal ablation in the rat brain using focused ultrasound and an ultrasound contrast agent: long-term effects. *J Neurosurg*. 2016; 125: 1539–48.
81. Miller DL, Lu X, Dou C, Zhu YI, Fuller R, Fields K, et al. Ultrasonic cavitation-enabled treatment for therapy of hypertrophic cardiomyopathy: Proof of principle. *Ultrasound Med Biol*. 2018; 44: 1439–50.
82. Tachibana K, Tachibana S. Albumin microbubble echo-contrast material as an enhancer for ultrasound accelerated thrombolysis. *Circulation*. 1995; 92: 1148–50.
83. Huynh E, Leung BYC, Helfield BL, Shakiba M, Gandier J-A, Jin CS, et al. In situ conversion of porphyrin microbubbles to nanoparticles for multimodality imaging. *Nat Nanotech*. 2015; 10: 325–32.
84. Blum NT, Yildirim A, Chattaraj R, Goodwin AP. Nanoparticles formed by acoustic destruction of microbubbles and their utilization for imaging and effects on therapy by high intensity focused ultrasound. *Theranostics*. 2017; 7: 694–702.
85. Tzu-Yin W, Wilson KE, Machtaler S, Willmann JK. Ultrasound and microbubble guided drug delivery: mechanistic understanding and clinical implications. *Curr Pharm Biotechnol*. 2013; 14: 743–52.
86. Lin C-Y, Li J-R, Tseng H-C, Wu M-F, Lin W-L. Enhancement of focused ultrasound with microbubbles on the treatments of anticancer nanodrug in mouse tumors. *Nanomedicine*. 2012; 8: 900–7.
87. Ho Y-J, Wang T-C, Fan C-H, Yeh C-K. Spatially uniform tumor treatment and drug penetration by regulating ultrasound with microbubbles. *ACS Appl Mater Interfaces*. 2018; 10: 17784–91.
88. Bazan-Peregrino M, Arvanitis CD, Rifai B, Seymour LW, Coussios C-C. Ultrasound-induced cavitation enhances the delivery and therapeutic efficacy of an oncolytic virus in an in vitro model. *J Control Release*. 2012; 157: 235–42.
89. Nakatsuka MA, Lee JH, Nakayama E, Hung AM, Hsu MJ, Mattrey RF, et al. Facile one-pot synthesis of polymer-phospholipid composite microbubbles with enhanced drug loading capacity for ultrasound-triggered therapy. *Soft Matter*. 2011; 7: 1656–9.
90. Kheirrolomoom A, Dayton PA, Lum AF, Little E, Paoli EE, Zheng H, et al. Acoustically-active microbubbles conjugated to liposomes: characterization of a proposed drug delivery vehicle. *Journal of Controlled Release*. 2007; 118: 275–84.
91. Yan F, Li L, Deng Z, Jin Q, Chen J, Yang W, et al. Paclitaxel-liposome-microbubble complexes as ultrasound-triggered therapeutic drug delivery carriers. *J Control Release*. 2013; 166: 246–55.
92. Geers B, Lentacker J, Sanders NN, Demeester J, Meairs S, De Smedt SC. Self-assembled liposome-loaded microbubbles: The missing link for safe and efficient ultrasound triggered drug-delivery. *J Control Release*. 2011; 152: 249–56.
93. Song K-H, Fan AC, Hinkle JJ, Newman J, Borden MA, Harvey BK. Microbubble gas volume: A unifying dose parameter in blood-brain barrier opening by focused ultrasound. *Theranostics*. 2017; 7: 144–52.
94. McMahon D, Hynynen K. Acute inflammatory response following increased blood-brain barrier permeability induced by focused ultrasound is dependent on microbubble dose. *Theranostics*. 2017; 7: 3989–4000.
95. Lipsman N, Meng Y, Bethune AJ, Huang Y, Lam B, Masellis M, et al. Blood-brain barrier opening in Alzheimer's disease using MR-guided focused ultrasound. *Nat Commun*. 2018 25; 9: 2336.
96. Kovacs ZI, Kim S, Jikaria N, Qureshi F, Milo B, Lewis BK, et al. Disrupting the blood-brain barrier by focused ultrasound induces sterile inflammation. *Proc Natl Acad Sci USA*. 2017; 114: E75–84.
97. Shi L, Palacio-Mancheno P, Badami J, Shin DW, Zeng M, Cardoso L, et al. Quantification of transient increase of the blood-brain barrier permeability to macromolecules by optimized focused ultrasound combined with microbubbles. *Int J Nanomedicine*. 2014; 9: 4437–48.
98. McDannold N, Vykhotseva N, Raymond S, Jolesz FA, Hynynen K. MRI-guided targeted blood-brain barrier disruption with focused ultrasound: Histological findings in rabbits. *Ultrasound Med Biol*. 2005; 31: 1527–37.
99. Sheikov N, McDannold N, Vykhotseva N, Jolesz F, Hynynen K. Cellular mechanisms of the blood-brain barrier opening induced by ultrasound in presence of microbubbles. *Ultrasound Med Biol*. 2004; 30: 979–89.

100. Sheikov N, McDannold N, Jolesz F, Zhang Y-Z, Tam K, Hynynen K. Brain arterioles show more active vesicular transport of blood-borne tracer molecules than capillaries and venules after focused ultrasound-evoked opening of the blood-brain barrier. *Ultrasound Med Biol.* 2006; 32: 1399–409.
101. Sheikov N, McDannold N, Sharma S, Hynynen K. Effect of focused ultrasound applied with an ultrasound contrast agent on the tight junctional integrity of the brain microvascular endothelium. *Ultrasound Med Biol.* 2008; 34: 1093–104.
102. Fan C-H, Ting C-Y, Liu H-L, Huang C-Y, Hsieh H-Y, Yen T-C, et al. Antiangiogenic-targeting drug-loaded microbubbles combined with focused ultrasound for glioma treatment. *Biomaterials.* 2013; 34: 2142–55.
103. Fan C-H, Ting C-Y, Lin H-J, Wang C-H, Liu H-L, Yen T-C, et al. SPIO-conjugated, doxorubicin-loaded microbubbles for concurrent MRI and focused-ultrasound enhanced brain-tumor drug delivery. *Biomaterials.* 2013; 34: 3706–15.
104. Zhao G, Huang Q, Wang F, Zhang X, Hu J, Tan Y, et al. Targeted shRNA-loaded liposome complex combined with focused ultrasound for blood brain barrier disruption and suppressing glioma growth. *Cancer Lett.* 2018; 418: 147–58.
105. Yue P, Miao W, Gao L, Zhao X, Teng J. Ultrasound-triggered effects of the microbubbles coupled to gdnf plasmid-loaded pegylated liposomes in a rat model of Parkinson's disease. *Front Neurosci.* 2018; 12: 222.
106. Fan C-H, Chang E-L, Ting C-Y, Lin Y-C, Liao E-C, Huang C-Y, et al. Folate-conjugated gene-carrying microbubbles with focused ultrasound for concurrent blood-brain barrier opening and local gene delivery. *Biomaterials.* 2016; 106: 46–57.
107. Zhang N, Yan F, Liang X, Wu M, Shen Y, Chen M, et al. Localized delivery of curcumin into brain with polysorbate 80-modified cerasomes by ultrasound-targeted microbubble destruction for improved Parkinson's disease therapy. *Theranostics.* 2018; 8: 2264–77.
108. Huang H-Y, Liu H-L, Hsu P-H, Chiang C-S, Tsai C-H, Chi H-S, et al. A multitheragnostic nanobubble system to induce blood-brain barrier disruption with magnetically guided focused ultrasound. *Adv Mater.* 2015; 27: 655–61.
109. Mulik RS, Bing C, Ladouceur-Wodzak M, Munaweera I, Chopra R, Corbin IR. Localized delivery of low-density lipoprotein docosahexaenoic acid nanoparticles to the rat brain using focused ultrasound. *Biomaterials.* 2016; 83: 257–68.
110. Coluccia D, Figueiredo CA, Wu MY, Riemenschneider AN, Diaz R, Luck A, et al. Enhancing glioblastoma treatment using cisplatin-gold-nanoparticle conjugates and targeted delivery with magnetic resonance-guided focused ultrasound. *Nanomedicine.* 2018; 14: 1137–48.
111. Timbie KF, Alzal U, Date A, Zhang C, Song J, Wilson Miller G, et al. MR image-guided delivery of cisplatin-loaded brain-penetrating nanoparticles to invasive glioma with focused ultrasound. *J Control Release.* 2017; 263: 120–31.
112. Mead BP, Kim N, Miller GW, Hodges D, Mastorakos P, Klivanov AL, et al. Novel focused ultrasound gene therapy approach noninvasively restores dopaminergic neuron function in a rat Parkinson's disease model. *Nano Lett.* 2017; 17: 3533–42.
113. Wu S-Y, Aurup C, Sanchez CS, Grondin J, Zheng W, Kamimura H, et al. Efficient blood-brain barrier opening in primates with neuronavigation-guided ultrasound and real-time acoustic mapping. *Sci Rep.* 2018; 8: 7978.
114. Sun T, Zhang Y, Power C, Alexander PM, Sutton JT, Aryal M, et al. Closed-loop control of targeted ultrasound drug delivery across the blood-brain/tumor barriers in a rat glioma model. *Proc Natl Acad Sci USA.* 2017; 114: E10281–90.
115. Garg S, Thomas AA, Borden MA. The effect of lipid monolayer in-plane rigidity on in vivo microbubble circulation persistence. *Biomaterials.* 2013; 34: 6862–70.
116. Chen CC, Sirsi SR, Homma S, Borden MA. Effect of surface architecture on in vivo ultrasound contrast persistence of targeted size-selected microbubbles. *Ultrasound Med Biol.* 2012; 38: 492–503.
117. Moyer LC, Timbie KF, Sheeran PS, Price RJ, Miller GW, Dayton PA. High-intensity focused ultrasound ablation enhancement in vivo via phase-shift nanodroplets compared to microbubbles. *J Ther Ultrasound.* 2015; 3: 7.
118. McDannold NJ, Vykhodtseva NI, Hynynen K. Microbubble contrast agent with focused ultrasound to create brain lesions at low power levels: MR imaging and histologic study in rabbits. *Radiology.* 2006; 241: 95–106.
119. Phillips LC, Puett C, Sheeran PS, Dayton PA, Wilson Miller G, Matsunaga TO. Phase-shift perfluorocarbon agents enhance high intensity focused ultrasound thermal delivery with reduced near-field heating. *J. Acoust. Soc. Am.* 2013; 134: 1473–82.
120. Sheeran PS, Dayton PA. Phase-change contrast agents for imaging and therapy. *Curr Pharm Des.* 2012; 18: 2152–65.
121. Sheeran PS, Rojas JD, Puett C, Hjelmquist J, Arena CB, Dayton PA. Contrast-enhanced ultrasound imaging and in vivo circulatory kinetics with low-boiling-point nanoscale phase-change perfluorocarbon agents. *Ultrasound Med Biol.* 2015; 41: 814–31.
122. Krippfgans OD, Fowlkes JB, Miller DL, Eldevik OP, Carson PL. Acoustic droplet vaporization for therapeutic and diagnostic applications. *Ultrasound Med Biol.* 2000; 26: 1177–89.
123. Zhang P, Porter T. An in vitro study of a phase-shift nanoemulsion: a potential nucleation agent for bubble-enhanced HIFU tumor ablation. *Ultrasound Med Biol.* 2010; 36: 1856–66.
124. Wang C-H, Kang S-T, Yeh C-K. Superparamagnetic iron oxide and drug complex-embedded acoustic droplets for ultrasound targeted theranosis. *Biomaterials.* 2013; 34: 1852–61.
125. Yan S, LU M, Ding X, Chen F, He X, Xu C, et al. HematoPorphyrin Monomethyl Ether polymer contrast agent for ultrasound/photoacoustic dual-modality imaging-guided synergistic high intensity focused ultrasound (HIFU) therapy. *Sci Rep.* 2016; 6: 31833.
126. You Y, Wang Z, Ran H, Zheng Y, Wang D, Xu J, et al. Nanoparticle-enhanced synergistic HIFU ablation and transarterial chemoembolization for efficient cancer therapy. *Nanoscale.* 2016; 8: 4324–39.
127. Aydin O, Vlaisavljevich E, Yuksel Durmaz Y, Xu Z, ElSayed MEH. Noninvasive ablation of prostate cancer spheroids using acoustically-activated nanodroplets. *Mol Pharm.* 2016; 13: 4054–65.
128. Yuksel Durmaz Y, Vlaisavljevich E, Xu Z, ElSayed M. Development of nanodroplets for histotripsy-mediated cell ablation. *Mol Pharm.* 2014; 11: 3684–95.
129. Kopeček JA, Park E-J, Zhang Y-Z, Vykhodtseva NI, McDannold NJ, Porter TM. Cavitation-enhanced MR-guided focused ultrasound ablation of rabbit tumors in vivo using phase shift nanoemulsions. *Phys Med Biol.* 2014; 59: 3465–81.
130. Pajek D, Burgess A, Huang Y, Hynynen K. High-intensity focused ultrasound sonothrombolysis: the use of perfluorocarbon droplets to achieve clot lysis at reduced acoustic power. *Ultrasound Med Biol.* 2014; 40: 2151–61.
131. Burgess A, Huang Y, Waspe AC, Ganguly M, Goertz DE, Hynynen K. High-intensity focused ultrasound (HIFU) for dissolution of clots in a rabbit model of embolic stroke. *PLoS One.* 2012; 7: e42311.
132. Kang S-T, Lin Y-C, Yeh C-K. Mechanical bioeffects of acoustic droplet vaporization in vessel-mimicking phantoms. *Ultrason Sonochem.* 2014; 21: 1866–74.
133. Lam RC, Shah S, Faries PL, McKinsey JF, Kent KC, Morrissey NJ. Incidence and clinical significance of distal embolization during percutaneous interventions involving the superficial femoral artery. *J Vasc Surg.* 2007; 46: 1155–9.
134. Henriques JPS, Zijlstra F, Ottervanger JP, de Boer M-J, van 't Hof AWJ, Hoorntje JCA, et al. Incidence and clinical significance of distal embolization during primary angioplasty for acute myocardial infarction. *Eur Heart J.* 2002; 23: 1112–7.
135. Limbruno U, De Carlo M, Pistolesi S, Micheli A, Sonia Petronio A, Camacci T, et al. Distal embolization during primary angioplasty: Histopathologic features and predictability. *Am Heart J.* 2005; 150: 102–8.
136. Nozari A, Dilekoz E, Sukhotinsky I, Stein T, Eikermann-Haerter K, Liu C, et al. Microemboli may link spreading depression, migraine aura, and patent foramen ovale. *Ann Neurol.* 2010; 67: 221–9.
137. Guo S, Du X, Wang X, Lu S, Shi A, Xu S, et al. Reduced clot debris size using standing waves formed via high intensity focused ultrasound. *Appl Phys Lett.* 2017; 111: 123701.
138. Maxwell AD, Cain CA, Duryea AP, Yuan L, Gurm HS, Xu Z. Noninvasive thrombolysis using pulsed ultrasound cavitation therapy - histotripsy. *Ultrasound Med Biol.* 2009; 35: 1982–94.
139. Wright C, Hynynen K, Goertz D. In vitro and in vivo high intensity focused ultrasound thrombolysis. *Invest Radiol.* 2012; 47: 217–25.
140. Xu S, Zong Y, Feng Y, Liu R, Liu X, Hu Y, et al. Dependence of pulsed focused ultrasound induced thrombolysis on duty cycle and cavitation bubble size distribution. *Ultrasonics Sonochem.* 2015; 22: 160–6.
141. Sehgal CM, Arger PH, Pugh CR. Sonographic enhancement of renal cortex by contrast media. *J Ultrasound Med.* 1995; 14: 749–50.
142. Forsberg F, Liu JB, Merton DA, Rawool NM, Goldberg BB. Parenchymal enhancement and tumor visualization using a new sonographic contrast agent. *J Ultrasound Med.* 1995; 14: 949–57.
143. Haworth KJ, Fowlkes JB, Carson PL, Krippfgans OD. Towards aberration correction of transcranial ultrasound using acoustic droplet vaporization. *Ultrasound Med Biol.* 2008; 34: 435–45.
144. Matsumura Y, Maeda H. A new concept for macromolecular therapeutics in cancer chemotherapy: mechanism of tumorotropic accumulation of proteins and the antitumor agent smancs. *Cancer Res.* 1986; 46: 6387–92.
145. Iyer AK, Khaled G, Fang J, Maeda H. Exploiting the enhanced permeability and retention effect for tumor targeting. *Drug Discov Today.* 2006; 11: 812–8.
146. Li M, Luo H, Zhang W, He K, Chen Y, Liu J, et al. Phase-shift, targeted nanoparticles for ultrasound molecular imaging by low intensity focused ultrasound irradiation. *Int J Nanomedicine.* 2018; 13: 3907–20.
147. Li DS, Yoon SJ, Pelivanov I, Frenz M, O'Donnell M, Pozzo LD. Polypyrrole-coated perfluorocarbon nanoemulsions as a sono-photoacoustic contrast agent. *Nano Lett.* 2017; 17: 6184–94.
148. Errico C, Pierre J, Pezet S, Desailly Y, Lenkei Z, Couture O, et al. Ultrafast ultrasound localization microscopy for deep super-resolution vascular imaging. *Nature.* 2015; 527: 499–502.
149. Hingot V, Bézagu M, Errico C, Desailly Y, Bocheux R, Tanter M, et al. Subwavelength far-field ultrasound drug-delivery. *Appl Phys Lett.* 2016; 109: 194102.
150. Rapoport N. Phase-shift, stimuli-responsive perfluorocarbon nanodroplets for drug delivery to cancer. *Wiley Interdiscip Rev Nanomed Nanobiotechnol.* 2012; 4: 492–510.

151. Bull JL. Cardiovascular bubble dynamics. *Crit Rev Biomed Eng.* 2005; 33: 299–346.
152. Chattaraj R, Goldscheitter GM, Yildirim A, Goodwin AP. Phase behavior of mixed lipid monolayers on perfluorocarbon nanoemulsions and its effect on acoustic contrast. *RSC Adv.* 2016; 6: 111318–25.
153. Chattaraj R, Mohan P, Besmer JD, Goodwin AP. Selective vaporization of superheated nanodroplets for rapid, sensitive, acoustic biosensing. *Adv Healthc Mater.* 2015; 4: 1790–5.
154. Shin SH, Park E-J, Min C, Choi SI, Jeon S, Kim Y-H, et al. Tracking perfluorocarbon nanoemulsion delivery by 19f mri for precise high intensity focused ultrasound tumor ablation. *Theranostics.* 2017; 7: 562–72.
155. Tirotta I, Dichiarante V, Pigiaccielli C, Cavallo G, Terraneo G, Bombelli FB, et al. 19F magnetic resonance imaging (MRI): from design of materials to clinical applications. *Chem Rev.* 2015; 115: 1106–29.
156. Yao M, Ma M, Xu H, Pan X, Xu G, Wu R. Small PLGA nanocapsules co-encapsulating copper sulfide nanodots and fluorocarbon compound for photoacoustic imaging-guided HIFU synergistic therapy. *RSC Adv.* 2018; 8: 4514–24.
157. Hannah AS, VanderLaan D, Chen Y-S, Emelianov SY. Photoacoustic and ultrasound imaging using dual contrast perfluorocarbon nanodroplets triggered by laser pulses at 1064 nm. *Biomed Opt Express.* 2014; 5: 3042–52.
158. Zhou D, Li C, He M, Ma M, Li P, Gong Y, et al. Folate-targeted perfluorohexane nanoparticles carrying bismuth sulfide for use in US/CT dual-mode imaging and synergistic high-intensity focused ultrasound ablation of cervical cancer. *J Mater Chem B.* 2016; 4: 4164–81.
159. Ho Y-J, Yeh C-K. Concurrent anti-vascular therapy and chemotherapy in solid tumors using drug-loaded acoustic nanodroplet vaporization. *Acta Biomater.* 2017; 49: 472–85.
160. Rapoport N, Nam K-H, Gupta R, Gao Z, Mohan P, Payne A, et al. Ultrasound-mediated tumor imaging and nanotherapy using drug loaded, block copolymer stabilized perfluorocarbon nanoemulsions. *J Control Release.* 2011; 153: 4–15.
161. Zhang L, Yin T, Li B, Zheng R, Qiu C, Lam KS, et al. Size-modulable nanoprobe for high-performance ultrasound imaging and drug delivery against cancer. *ACS Nano.* 2018; 12: 3449–60.
162. Zhang X, Zheng Y, Wang Z, Huang S, Chen Y, Jiang W, et al. Methotrexate-loaded PLGA nanobubbles for ultrasound imaging and Synergistic Targeted therapy of residual tumor during HIFU ablation. *Biomaterials.* 2014; 35: 5148–61.
163. Gao D, Xu M, Cao Z, Gao J, Chen Y, Li Y, et al. Ultrasound-triggered phase-transition cationic nanodroplets for enhanced gene delivery. *ACS Appl Mater Interfaces.* 2015; 7: 13524–37.
164. Burgess MT, Porter TM. Acoustic cavitation-mediated delivery of small interfering ribonucleic acids with phase-shift nano-emulsions. *Ultrasound Med Biol.* 2015; 41: 2191–201.
165. Fabiilli ML, Lee JA, Kripfgans OD, Carson PL, Fowlkes JB. Delivery of water-soluble drugs using acoustically triggered perfluorocarbon double emulsions. *Pharm Res.* 2010; 27: 2753–65.
166. Duncanson WJ, Arriaga LR, Ung WL, Kopeček JA, Porter TM, Weitz DA. Microfluidic fabrication of perfluorohexane-shelled double emulsions for controlled loading and acoustic-triggered release of hydrophilic agents. *Langmuir.* 2014; 30: 13765–70.
167. Ibsen S, Benchimol M, Simberg D, Schutt C, Steiner J, Esener S. A novel nested liposome drug delivery vehicle capable of ultrasound triggered release of its payload. *J Control Release.* 2011; 155: 358–66.
168. Ho Y-J, Yeh C-K. Theranostic performance of acoustic nanodroplet vaporization-generated bubbles in tumor intertissue. *Theranostics.* 2017; 7: 1477–88.
169. Brown JM, Wilson WR. Exploiting tumour hypoxia in cancer treatment. *Nat Rev Cancer.* 2004; 4: 437–47.
170. Wilson WR, Hay MP. Targeting hypoxia in cancer therapy. *Nat Rev Cancer.* 2011; 11: 393–410.
171. Magnetto C, Prato M, Khadjavi A, Giribaldi G, Fenoglio I, Jose J, et al. Ultrasound-activated decafluoropentane-cored and chitosan-shelled nanodroplets for oxygen delivery to hypoxic cutaneous tissues. *RSC Adv.* 2014; 4: 38433–41.
172. Cheng Y, Cheng H, Jiang C, Qiu X, Wang K, Huan W, et al. Perfluorocarbon nanoparticles enhance reactive oxygen levels and tumour growth inhibition in photodynamic therapy. *Nat Commun.* 2015; 6: 8785.
173. Song X, Feng L, Liang C, Yang K, Liu Z. Ultrasound triggered tumor oxygenation with oxygen-shuttle nanoparticle to overcome hypoxia-associated resistance in cancer therapies. *Nano Lett.* 2016; 16: 6145–53.
174. Stylianopoulos T, Jain RK. Design considerations for nanotherapeutics in oncology. *Nanomedicine.* 2015; 11: 1893–907.
175. Jain RK, Stylianopoulos T. Delivering nanomedicine to solid tumors. *Nat Rev Clin Oncol.* 2010; 7: 653–64.
176. Danhier F. To exploit the tumor microenvironment: Since the EPR effect fails in the clinic, what is the future of nanomedicine? *J Control Release.* 2016 28; 244: 108–21.
177. Choi M-R, Stanton-Maxey KJ, Stanley JK, Levin CS, Bardhan R, Akin D, et al. A cellular Trojan Horse for delivery of therapeutic nanoparticles into tumors. *Nano Lett.* 2007; 7: 3759–65.
178. Huang W-C, Chiang W-H, Cheng Y-H, Lin W-C, Yu C-F, Yen C-Y, et al. Tumor-tropic monocyte-mediated delivery of echogenic polymer bubbles and therapeutic vesicles for chemotherapy of tumor hypoxia. *Biomaterials.* 2015; 71: 71–83.
179. Wang X, Chen H, Chen Y, Ma M, Zhang K, Li F, et al. Perfluorohexane-encapsulated mesoporous silica nanocapsules as enhancement agents for highly efficient high intensity focused ultrasound (HIFU). *Adv Mater.* 2012; 24: 785–91.
180. Zhang N, Cai X, Gao W, Wang R, Xu C, Yao Y, et al. A multifunctional theranostic nanoagent for dual-mode image-guided HIFU/chemo- synergistic cancer therapy. *Theranostics.* 2016; 6: 404–17.
181. Martínez HP, Kono Y, Blair SL, Sandoval S, Wang-Rodríguez J, Mattrey RF, et al. Hard shell gas-filled contrast enhancement particles for colour Doppler ultrasound imaging of tumors. *Med Chem Comm.* 2010; 1: 266–70.
182. Yang P, Wang F, Luo X, Zhang Y, Guo J, Shi W, et al. Rational design of magnetic nanorattles as contrast agents for ultrasound/magnetic resonance dual-modality imaging. *ACS Appl Mater Interfaces.* 2014; 6: 12581–7.
183. Wang J, Barback CV, Ta CN, Weeks J, Gude N, Mattrey RF, et al. Extended lifetime in vivo pulse stimulated ultrasound imaging. *IEEE Trans Med Imaging.* 2018; 37: 222–9.
184. Ma M, Xu H, Chen H, Jia X, Zhang K, Wang Q, et al. A drug-perfluorocarbon nanoemulsion with an ultrathin silica coating for the synergistic effect of chemotherapy and ablation by high-intensity focused ultrasound. *Adv Mater.* 2014; 26: 7378–85.
185. Zhang K, Chen H, Li F, Wang Q, Zheng S, Xu H, et al. A continuous tri-phase transition effect for HIFU-mediated intravenous drug delivery. *Biomaterials.* 2014; 35: 5875–85.
186. Ma M, Yan F, Yao M, Wei Z, Zhou D, Yao H, et al. Template-free synthesis of hollow/porous organosilica-Fe₃O₄ hybrid nanocapsules toward magnetic resonance imaging-guided high-intensity focused ultrasound therapy. *ACS Appl Mater Interfaces.* 2016; 8: 29986–96.
187. Yildirim A, Chattaraj R, Blum NT, Goldscheitter GM, Goodwin AP. Stable encapsulation of air in mesoporous silica nanoparticles: Fluorocarbon-free nanoscale ultrasound contrast agents. *Adv Healthc Mater.* 2016; 5: 1290–8.
188. Kwan JJ, Myers R, Coviello CM, Graham SM, Shah AR, Stride E, et al. Ultrasound-propelled nanocapsules for drug delivery. *Small.* 2015; 11: 5305–14.
189. Zhang L, Belova V, Wang H, Dong W, Möhwald H. Controlled cavitation at nano/microparticle surfaces. *Chem Mater.* 2014; 26: 2244–8.
190. Jin Q, Kang S-T, Chang Y-C, Zheng H, Yeh C-K. Inertial cavitation initiated by polytetrafluoroethylene nanoparticles under pulsed ultrasound stimulation. *Ultrasound Sonochem.* 2016; 32: 1–7.
191. Zhao Y, Zhu Y, Fu J, Wang L. Effective cancer cell killing by hydrophobic nanovoid-enhanced cavitation under safe low-energy ultrasound. *Chem Asian J.* 2014; 9: 790–6.
192. Jin Q, Lin C-Y, Chang Y-C, Yang C-M, Yeh C-K. Roles of textural and surface properties of nanoparticles in ultrasound-responsive systems. *Langmuir.* 2018; 34: 1256–65.
193. Kwan JJ, Lajoie G, de Jong N, Stride E, Versluis M, Coussios CC. Ultrahigh-speed dynamics of micrometer-scale inertial cavitation from nanoparticles. *Phys Rev Applied.* 2016; 6: 044004.
194. Yildirim A, Chattaraj R, Blum NT, Shi D, Kumar K, Goodwin AP. Phospholipid capped mesoporous nanoparticles for targeted high intensity focused ultrasound ablation. *Adv Healthc Mater.* 2017; 6: 1700514.
195. Yildirim A, Chattaraj R, Blum NT, Goodwin AP. Understanding acoustic cavitation initiation by porous nanoparticles: toward nanoscale agents for ultrasound imaging and therapy. *Chem Mater.* 2016; 28: 5962–72.
196. Paris JL, Mannaris C, Cabañas MV, Carlisle R, Manzano M, Vallet-Regí M, et al. Ultrasound-mediated cavitation-enhanced extravasation of mesoporous silica nanoparticles for controlled-release drug delivery. *Chem Eng J.* 2018; 340: 2–8.
197. Mannaris C, Teo BM, Seth A, Bau L, Coussios C, Stride E. Gas-stabilizing gold nanocones for acoustically mediated drug delivery. *Adv Healthc Mater.* 2018; 7: e1800184.
198. Myers R, Grundy M, Rowe C, Coviello CM, Bau L, Erbs P, et al. Ultrasound-mediated cavitation does not decrease the activity of small molecule, antibody or viral-based medicines. *Int J Nanomedicine.* 2018; 13: 337–49.
199. Wang Z, Qiao R, Tang N, Lu Z, Wang H, Zhang Z, et al. Active targeting theranostic iron oxide nanoparticles for MRI and magnetic resonance-guided focused ultrasound ablation of lung cancer. *Biomaterials.* 2017; 127: 25–35.
200. Józefczak A, Kaczmarek K, Hornowski T, Kubovčková M, Rozynek Z, Timko M, et al. Magnetic nanoparticles for enhancing the effectiveness of ultrasonic hyperthermia. *Appl Phys Lett.* 2016; 108: 263701.
201. Kaczmarek K, Hornowski T, Dobosz B, Józefczak A. Influence of Magnetic Nanoparticles on the Focused Ultrasound Hyperthermia. *Materials.* 2018; 11: e1607.
202. McLaughlan JR, Roy RA, Ju H, Murray TW. Ultrasonic enhancement of photoacoustic emissions by nanoparticle-targeted cavitation. *Opt Lett.* 2010; 35: 2127–9.
203. Kang E, Min HS, Lee J, Han MH, Ahn HJ, Yoon I-C, et al. Nanobubbles from gas-generating polymeric nanoparticles: ultrasound imaging of living subjects. *Angew Chem Int Ed.* 2010; 49: 524–8.
204. Min KH, Min HS, Lee HJ, Park DJ, Yhee JY, Kim K, et al. pH-controlled gas-generating mineralized nanoparticles: a theranostic agent for ultrasound imaging and therapy of cancers. *ACS Nano.* 2015; 9: 134–45.

205. Min HS, Son S, You DG, Lee TW, Lee J, Lee S, et al. Chemical gas-generating nanoparticles for tumor-targeted ultrasound imaging and ultrasound-triggered drug delivery. *Biomaterials*. 2016; 108: 57–70.
206. Kang C, Cho W, Park M, Kim J, Park S, Shin D, et al. H₂O₂-triggered bubble generating antioxidant polymeric nanoparticles as ischemia/reperfusion targeted nanotheranostics. *Biomaterials*. 2016; 85: 195–203.
207. Liu T, Zhang N, Wang Z, Wu M, Chen Y, Ma M, et al. Endogenous catalytic generation of O₂ bubbles for in situ ultrasound-guided high intensity focused ultrasound ablation. *ACS Nano*. 2017; 11: 9093–102.
208. Feng G, Hao L, Xu C, Ran H, Zheng Y, Li P, et al. High-intensity focused ultrasound-triggered nanoscale bubble-generating liposomes for efficient and safe tumor ablation under photoacoustic imaging monitoring. *Int J Nanomedicine*. 2017; 12: 4647–59.
209. Zhang K, Xu H, Jia X, Chen Y, Ma M, Sun L, et al. Ultrasound-triggered nitric oxide release platform based on energy transformation for targeted inhibition of pancreatic tumor. *ACS Nano*. 2016; 10: 10816–28.
210. Santos MA, Goertz DE, Hynynen K. Focused ultrasound hyperthermia mediated drug delivery using thermosensitive liposomes and visualized with in vivo two-photon microscopy. *Theranostics*. 2017; 7: 2718–31.
211. Dromi S, Frenkel V, Luk A, Traugher B, Angstadt M, Bur M, et al. Pulsed-high intensity focused ultrasound and low temperature-sensitive liposomes for enhanced targeted drug delivery and antitumor effect. *Clin Cancer Res*. 2007; 13: 2722–7.
212. Park SM, Kim MS, Park S-J, Park ES, Choi K-S, Kim Y-S, et al. Novel temperature-triggered liposome with high stability: formulation, in vitro evaluation, and in vivo study combined with high-intensity focused ultrasound (HIFU). *J Control Release*. 2013; 170: 373–9.
213. Liang X, Gao J, Jiang L, Luo J, Jing L, Li X, et al. Nanohybrid liposomal cerasomes with good physiological stability and rapid temperature responsiveness for high intensity focused ultrasound triggered local chemotherapy of cancer. *ACS Nano*. 2015; 9: 1280–93.
214. Wu P, Jia Y, Qu F, Sun Y, Wang P, Zhang K, et al. Ultrasound-responsive polymeric micelles for sonoporation-assisted site-specific therapeutic action. *ACS Appl Mater Interfaces*. 2017; 9: 25706–16.
215. Deckers R, Paradissis A, Oerlemans C, Talelli M, Storm G, Hennink WE, et al. New insights into the HIFU-triggered release from polymeric micelles. *Langmuir*. 2013; 29: 9483–90.
216. Li W, Cai X, Kim C, Sun G, Zhang Y, Deng R, et al. Gold nanocages covered with thermally-responsive polymers for controlled release by high-intensity focused ultrasound. *Nanoscale*. 2011; 3: 1724–30.
217. Wang J, Pelletier M, Zhang H, Xia H, Zhao Y. High-frequency ultrasound-responsive block copolymer micelle. *Langmuir*. 2009; 25: 13201–5.
218. Tong R, Lu X, Xia H. A facile mechanophore functionalization of an amphiphilic block copolymer towards remote ultrasound and redox dual stimulus responsiveness. *Chem Commun*. 2014; 50: 3575–8.
219. O'Neill HS, Herron CC, Hastings CL, Deckers R, Lopez Noriega A, Kelly HM, et al. A stimuli responsive liposome loaded hydrogel provides flexible on-demand release of therapeutic agents. *Acta Biomater*. 2017; 48: 110–9.
220. López-Noriega A, Hastings CL, Ozbakir B, O'Donnell KE, O'Brien FJ, Storm G, et al. Hyperthermia-induced drug delivery from thermosensitive liposomes encapsulated in an injectable hydrogel for local chemotherapy. *Adv Health Mater*. 2014; 3: 854–9.
221. Moncion A, Lin M, O'Neill EG, Franceschi RT, Kripfgans OD, Putnam AJ, et al. Controlled release of basic fibroblast growth factor for angiogenesis using acoustically-responsive scaffolds. *Biomaterials*. 2017; 140: 26–36.
222. Moncion A, Arlotta KJ, O'Neill EG, Lin M, Mohr LA, Franceschi RT, et al. In vitro and in vivo assessment of controlled release and degradation of acoustically responsive scaffolds. *Acta Biomater*. 2016; 46: 221–33.
223. Fabiilli ML, Wilson CG, Padilla F, Martin-Saavedra FM, Fowlkes JB, Franceschi RT. Acoustic droplet-hydrogel composites for spatial and temporal control of growth factor delivery and scaffold stiffness. *Acta Biomater*. 2013; 9: 7399–409.
224. Moncion A, Arlotta KJ, Kripfgans OD, Fowlkes JB, Carson PL, Putnam AJ, et al. Design and characterization of fibrin-based acoustically responsive scaffolds for tissue engineering applications. *Ultrasound Med Biol*. 2016; 42: 257–71.
225. Soto F, Martin A, Ibsen S, Vaidyanathan M, Garcia-Gradilla V, Levin Y, et al. Acoustic microcannons: Toward advanced microballistics. *ACS Nano*. 2016; 10: 1522–8.
226. Soto F, Mishra RK, Chrostowski R, Martin A, Wang J. Epidermal tattoo patch for ultrasound-based transdermal microballistic delivery. *Adv Mater Technol*. 2017; 2: 1700210.
227. Soto F, Jeerapan I, Silva-López C, Lopez-Ramirez MA, Chai I, Xiaolong L, et al. Noninvasive transdermal delivery system of lidocaine using an acoustic droplet-vaporization based wearable patch. *Small*. 2018; 14: 1803266.
228. Yohe ST, Kopeček JA, Porter TM, Colson YL, Grinstaff MW. Triggered drug release from superhydrophobic meshes using high-intensity focused ultrasound. *Adv Health Mater*. 2013; 2: 1204–8.
229. Wang S, Zhao J, Hu F, Li X, An X, Zhou S, et al. Phase-changeable and bubble-releasing implants for highly efficient HIFU-responsive tumor surgery and chemotherapy. *J Mater Chem B*. 2016; 4: 7368–78.
230. Gai M, Frueh J, Tao T, Petrov AV, Petrov VV, Shesterikov EV, et al. Poly(lactic acid) nano- and microchamber arrays for encapsulation of small hydrophilic molecules featuring drug release via high intensity focused ultrasound. *Nanoscale*. 2017; 9: 7063–70.
231. Niu D, Wang X, Li Y, Zheng Y, Li F, Chen H, et al. Facile synthesis of magnetite/perfluorocarbon co-loaded organic/inorganic hybrid vesicles for dual-modality ultrasound/magnetic resonance imaging and imaging-guided high-intensity focused ultrasound ablation. *Adv Mater*. 2013; 25: 2686–92.
232. Chen H, Zhang W, Zhu G, Xie J, Chen X. Rethinking cancer nanotheranostics. *Nat Rev Mater*. 2017; 2: 17024.
233. Junttila MR, de Sauvage FJ. Influence of tumour micro-environment heterogeneity on therapeutic response. *Nature*. 2013; 501: 346–54.
234. Alizadeh AA, Aranda V, Bardelli A, Blanpain C, Bock C, Borowski C, et al. Toward understanding and exploiting tumor heterogeneity. *Nat Med*. 2015; 21: 846–53.
235. Mu Q, Jiang G, Chen L, Zhou H, Fourches D, Tropsha A, et al. Chemical basis of interactions between engineered nanoparticles and biological systems. *Chem Rev*. 2014; 114: 7740–81.
236. McNeil SE. Evaluation of nanomedicines: stick to the basics. *Nat Rev Mater*. 2016; 1: 16073.
237. Lammers T, Kiessling F, Ashford M, Hennink W, Crommelin D, Storm G. Cancer nanomedicine: is targeting our target? *Nat Rev Mater*. 2016; 1: 16069.
238. Faria M, Björnmalin M, Thurecht KJ, Kent SJ, Parton RG, Kavallaris M, et al. Minimum information reporting in bio-nano experimental literature. *Nat Nanotechnol*. 2018; 13: 777–85.
239. Pettitt ME, Lead JR. Minimum physicochemical characterisation requirements for nanomaterial regulation. *Environ Int*. 2013; 52: 41–50.